Isothermal compression of an eclogite from the Western Gneiss Region (Norway)

Martin Simon, Pavel Pitra, Philippe Yamato, Marc Poujol

Pitra Pavel (Orcid ID: 0000-0002-0462-2742)

Isothermal compression of an eclogite from the Western Gneiss Region (Norway)

Martin Simon[1], Pavel Pitra[1,2], Philippe Yamato[1,3], and Marc Poujol[1]

[1]Univ Rennes, CNRS, Géosciences Rennes, UMR 6118, 35000 Rennes, France

[2]Česká Geologická Služba, Praha 1, Česká republika

[3]Institut Universitaire de France (IUF), Paris, France

Corresponding author: martin.simon@univ-rennes1.fr

Co-authors: pavel.pitra@univ-rennes1.fr ; philippe.yamato@gmail.com ; marc.poujol@univ-rennes1.fr

Running title: Isothermal compression of an eclogite

Conflict of interest: The authors declare no conflict of interest.

Abstract

In the Western Gneiss Region in Norway, mafic eclogites form lenses within granitoid orthogneiss and contain the best record of the pressure and temperature evolution of this ultrahigh-pressure (UHP) terrane. Their exhumation from the UHP conditions has been extensively studied, but their prograde evolution has been rarely quantified although it represents a key constraint for the tectonic history of this area. This study focused on a well-preserved phengite-bearing eclogite sample from the Nordfjord region. The sample was investigated using phase-equilibrium modelling, trace-element analyses of garnet, trace- and major-element thermo-barometry and quartz-in-garnet barometry by Raman spectroscopy. Inclusions in garnet core point to crystallisation conditions in the amphibolite facies at 510–600 °C and 11–16 kbar, while chemical zoning in garnet suggests growth during isothermal compression up to the peak pressure of 28 kbar at 600 °C, followed by near-isobaric heating to 660–680 °C. Near-isothermal decompression to 10–14 kbar is recorded in fine-grained clinopyroxene-amphibole-plagioclase symplectites. The absence of a temperature increase

This article has been accepted for publication and undergone full peer review but has not been through the copyediting, typesetting, pagination and proofreading process which may lead to differences between this version and the Version of Record. Please cite this article as doi: 10.1002/jmg.12692

during compression seems incompatible with the classic view of crystallization along a geothermal gradient in a subduction zone and may question the tectonic significance of eclogite-facies metamorphism. Two end-member tectonic scenarios are proposed to explain such an isothermal compression: (1) either the mafic rocks were originally at depth within the lower crust and were consecutively buried along the isothermal portion of the subducting slab, or (2) the mafic rocks recorded up to 14 kbar of tectonic overpressure at constant depth and temperature during the collisional stage of the orogeny.

Keywords: UHP eclogite, Western Gneiss Region, Raman spectroscopy, pseudosections, non-lithostatic pressure

1. Introduction

Geodynamic reconstructions of former subduction zones and collisional orogens requires knowledge of the evolution of the involved rocks in terms of pressure (*P*) and temperature (*T*). Eclogites are widely studied to this end as, in general, they bear the best records of the metamorphic history at high pressures, although it is rare to have access to the full record from the prograde to the retrograde conditions. Indeed, the markers of the early orogenic stages are commonly erased by late recrystallization.

The Western Gneiss Region (WGR) in Norway (Figure 1) is a basement window through the stack of thrust nappes (so-called allochthons) resulting from the subduction of Baltica under Laurentia and their subsequent collision during the Caledonian orogeny. In the WGR, mafic eclogites are found both in the Baltica basement and in the lower nappes. The discovery of coesite (Smith, 1984) and microdiamond (Dobrzhinetskaya et al., 1995) led to the characterization of the WGR as one of the best-preserved ultrahigh-pressure (UHP) units on Earth. Many studies focused on the exhumation mechanisms of the eclogites and hence the post-peak-pressure part of their *P–T* evolution (Andersen, 1998; Andersen et al., 1991; Carswell, Brueckner, et al., 2003; Dewey et al., 1993; Fossen & Dallmeyer, 1998; Schärer & Labrousse, 2003; Labrousse et al., 2004; Root et al., 2004; Young et al., 2007; Johnston, Hacker, & Ducea, 2007; Labrousse et al., 2011). Consequently, there is a large dataset of *P–T* estimates (and associated *P–T* paths) for the peak and retrograde conditions (blue and grey ellipses respectively, Figure 2), whereas only very few data are available for the prograde, subduction-related, part of the history (green ellipses, Figure 2).

Based on metamorphic data from the allochthons (Hacker & Gans, 2005), Hacker et al. (2010) suggested that the UHP metamorphism was preceded by upper amphibolite-facies metamorphism along a Barrovian gradient (8–14 kbar, 500–700 °C). However, such metamorphism has not yet been described in the Baltica basement and the mafic bodies it contains; the transposition to this

basement of a *P–T* evolution inferred from units in a structurally different position, such as the allochthons, is arguable. In the Nordfjord-Stadlandet region, the rare existing data on the prograde history of the eclogites (Krogh, 1982; Schärer & Labrousse, 2003) do not concur (Figure 2), preventing their integration in any geodynamic reconstruction of the orogen. It is nevertheless of the utmost importance to constrain the *P–T* variations recorded in the rocks, as they are a first-order parameter in understanding the mechanisms that controlled the Caledonian orogeny.

In order to document the *P–T* evolution in the basement, we investigated a well-preserved eclogite with only minor retrogression from the Nordfjord-Stadlandet region using thermodynamic phase-equilibrium modelling, Raman spectroscopy on quartz inclusions in garnet, major- and trace-element thermobarometry and trace-element analyses of garnet. Our results reveal that both compression and retrogression occurred roughly isothermally and allow us to discuss the tectonic processes involved in the eclogite formation.

2. Geological setting

2.1. The Western Gneiss Region

The Caledonian orogeny resulted from the closure of the Iapetus Ocean and the subsequent collision between Baltica and Laurentia. This orogeny occurred in several phases between the Late Cambrian and the Early Devonian (see the summary in Roberts, 2003). In the early stages, important thrusting of different units occurred southeastwards (present-day coordinates), accommodating a shortening over several hundreds of kilometres (Gee, 1975; Roberts & Gee, 1985). From the base to the top (Figure 1a), these terranes are: the Lower and the Middle Allochthons, which represent the Balto-Scandian margin; the Upper Allochthon, with an oceanic affinity and derived from the Iapetus Ocean; and the Uppermost Allochthon, which shows evidence for Laurentian-derived terranes (Stephens & Gee, 1989; Roberts et al., 2002). During the Late Silurian–Early Devonian, known as the Scandian stage of the orogeny (Gee, 1975), the continuation of subduction of Baltica led to the burial of its basement together with part of the overlying nappes (see the review by Gee et al., 2013). Subsequent exhumation has been largely attributed to the eduction of the subducted continental crust, caused by the loss of the down-pulling oceanic slab (e.g. Andersen et al., 1991; Fossen, 1992; Andersen, 1998; Duretz et al., 2012; Wiest et al., 2021). Subsequent extensional collapse was accompanied by the development of crustal shear zones, as the top-to-the-West Nordfjord-Sogn Detachment Zone (NSDZ, see Figure 1; Andersen & Jamtveit, 1990; Krabbendam & Dewey, 1998; Hacker et al., 2003; Johnston, Hacker, & Andersen, 2007). Extension continued during the Devonian with normal and strike-slip faulting allowing the establishment of the Hornelen basin, filled with Old

Red Sandstone molasse overlying the study area (Figure 1c). The WGR hence corresponds to an erosional and tectonic window through the allochthon nappe stack.

The Western Gneiss Region consists mostly of coarse-grained granodioritic gneiss and granitic augengneiss, namely the Western Gneiss Complex (Gjelsvik, 1951; Bryhni, 1966). The protoliths of these rocks are ca. 1600 Ma old (i.e. Gothian age) and were affected by a first amphibolite- to granulite-facies metamorphism at ca. 950 Ma (Sveconorwegian orogeny), with *P*–*T* conditions around 9–11 kbar and 700–900 °C (e.g. Krabbendam et al., 2000; Wain et al., 2001; Corfu & Andersen, 2002; Root et al., 2005; Bingen et al., 2008). Other minor rock types present in the WGR are quartzite, carbonate and mica-schist. Various mafic and ultramafic bodies can be found throughout the WGR as metre- to kilometre-long lenses and boudins, representing only a small proportion of the total rock volume (~2 %; Peterman et al., 2009). They are metamorphosed to various degrees (mostly amphibolite- to eclogite facies), with lenses of contrastingly transformed rocks in the vicinity of one another (Straume & Austrheim, 1999; Krabbendam et al., 2000). (Ultra)mafic rocks have either a mantle origin, for the pyroxenite and peridotite lenses, or a crustal one; the latter are often referred to as external eclogites (for a summary of the controversy on the origin of the mafic bodies in the WGR, see Brueckner, 2018). These external eclogites have various protoliths, from mafic sills and dykes to mafic volcanic rocks (Bryhni, 1966). Traces of melting (leucosomes and granitic dykes) are found throughout the WGR and show various relationships with the eclogitic or amphibolitic fabrics of the host rocks, from concordant to discordant, which argue for partial melting occurring at different stages of the *P*–*T* evolution (Labrousse et al., 2004; Kylander-Clark & Hacker, 2014; Ganzhorn et al., 2014).

2.2 Caledonian metamorphism

The mafic bodies record a regional-scale progressive increase of temperature towards the NW (Krogh, 1977; Griffin et al., 1985). The presence of coesite or polycrystalline quartz interpreted as former coesite (Smith, 1984; Smith & Lappin, 1989; Wain, 1997; Carswell et al., 1999; Carswell, Tucker, et al., 2003) and microdiamond (Dobrzhinetskaya et al., 1995; van Roermund et al., 2002; Vrijmoed et al., 2008) testifies to UHP conditions. Eclogite-facies minerals are rarely recognized in the quartz-feldspathic lithologies except at the interface with the eclogitized mafic bodies (Engvik & Andersen, 2000; Wain et al., 2000).

The occurrences of coesite in the eclogites led to the definition of three specific UHP zones in the WGR (Figure 1b): the Nordfjord-Stadlandet zone (Wain, 1997; Cuthbert et al., 2000; Walsh & Hacker, 2004), the Sørøyane zone (Carswell et al., 2003; Root et al., 2005) and the Nordøyane zone (Terry et al., 2000; Vrijmoed et al., 2006). In the Nordfjord-Stadlandet region, eclogites within the UHP zone

mostly contain unzoned garnets with UHP inclusions, whereas outside the UHP zone, eclogites have zoned garnets with amphibolite-facies inclusions (Bryhni & Griffin, 1971; Wain, 1997; Cuthbert et al., 2000). Structural studies show that the UHP zones correspond to antiforms formed during late regional-scale folding (e.g. Root et al., 2005; Young, 2018), as highlighted by the shape of the regional isobars (Figure 1b). Occurrences of eclogite have also been found in the surrounding Lower and Middle allochthons, both in the hanging wall of the NSDZ (Johnston, Hacker, & Ducea, 2007; Young et al., 2007), in the allochthons to the east and the north of the study area, mostly in the Seve Nappe Complex (e.g. Walsh & Hacker, 2004; Hollocher et al., 2007; Janák et al., 2012; Beckman et al., 2014; Klonowska et al., 2016) and to the south in the Bergen Arcs (e.g. Austrheim, 1987; Jamtveit et al., 2018). In the WGR, eclogite-facies records are common and widespread but represent less than 2 % of the total rock volume (Peterman et al., 2009). The rest of the WGR and nearby allochthons show amphibolite- to granulite-facies *P*–*T* conditions between 500–800 °C and 5–15 kbar (Chauvet et al., 1992; Wilks & Cuthbert, 1994; Krabbendam & Wain, 1997; Engvik & Andersen, 2000; Labrousse et al., 2004; Walsh & Hacker, 2004; Hacker & Gans, 2005; Johnston, Hacker, & Ducea, 2007), interpreted either as metastable relics that remained untransformed during the Scandian metamorphic phase (60–70 %), or as the result of the post eclogite-facies reequilibration (~30 %; Peterman et al., 2009).

In the Nordfjord-Stadlandet zone, the metamorphic conditions before the eclogite-facies metamorphism are largely unknown. Based on the assemblage included in the garnet core of an eclogitic sample from Drage, Schärer & Labrousse (2003) determined that the pre-eclogite-facies conditions were 650±30 °C and 18.5±3.5 kbar (Figure 2). Also based on garnet inclusions, Krogh (1982) estimated epidote-amphibolite-facies conditions at 550–650 °C and 7–9 kbar for an eclogite from Verpeneset. Eclogite peak *P*–*T* conditions range widely, from 575 to 800 °C and 20 to 36 kbar. The conditions during the amphibolite-facies overprint were extensively reviewed by Labrousse et al. (2004), with retrogressed eclogites mostly yielding *P*–*T* conditions of 4–13 kbar and 550–650 °C. The host gneisses yield similar *P*–*T* conditions (Schärer & Labrousse, 2003; Labrousse et al., 2004; Peterman et al., 2009), up to ~720 °C and 14 kbar (Figure 2). Carter et al. (2021) suggested that symplectites in mafic eclogites from the Stadlandet peninsula formed during a two-stage retrogression, with isothermal decompression from UHP to 10–15 kbar at 650–700 °C followed by cooling and exhumation, down to 470 °C and 3 kbar.

2.3. The Vågsøy island

The studied eclogite sample was collected in Vågsvåg, in the southern part of the Vågsøy island, which has been less studied than the nearby eclogites from Stadlandet, Verpeneset, Kråkeneset or

Flatraket (Figure 1b). As the Nordfjord-Stadlandet UHP zone is mostly delineated by the presence of coesite or pseudomorphs after coesite (Wain, 1997; Cuthbert et al., 2000), precise *P–T* conditions are not available for all of the eclogites inventoried on Figure 1b. Labrousse et al. (2004) determined peak conditions of 645±50 °C and 21±2.5 kbar for a phengite-bearing eclogite from Vågsvåg. Decompression conditions were determined for the symplectite assemblage at 550–620 °C and 8.7–12.6 kbar. Krogh Ravna & Terry (2004) calculated the peak conditions at 29±3 kbar and 729±80 °C for an eclogite from Halnes (2 km southeast of Vågsvåg). Griffin & Brueckner (1985) obtained a Sm–Nd age of 423±12 Ma for a quartz- and rutile-bearing eclogite located in Raudeberg (7 km north of Vågsvåg). Kylander-Clark & Hacker (2014) obtained a zircon U–Pb age of 389±2 Ma for the emplacement of a granitic pegmatite, interpreted to reflect dehydration melting during the decompression from (U)HP to amphibolite-facies conditions. Spencer et al. (2013) interpreted similarly an epidote-bearing granitic leucosome cross-cutting both eclogitic and amphibolitic fabrics, from which they reported a titanite U–Pb age of 387±4 Ma with a crystallization temperature of 700 °C obtained using the Zr-in-rutile geothermometer.

3. Methods

3.1. Major-element chemical composition

The studied sample, free of any weathered material, was first crushed in an agate mortar to obtain a fine powder. Bulk-rock composition was determined by Inductively Coupled Plasma Optical Emission Spectrometry (ICP-OES) at the Centre of Petrographic and Geochemical Research (SARM laboratories, CRPG, CNRS, Nancy, France). Detailed analytical procedure can be found in Carignan et al. (2001). FeO vs total Fe_2O_3 was obtained by wet titration. The chemical composition of the sample is reported in Table S1.

Mineral analyses were performed with a Cameca SX100 electron microprobe (Microsonde Ouest, IFREMER Brest, France) in the wavelength dispersive mode. Operating conditions for the spot analyses were 15 keV accelerating voltage, 20 nA beam current, 10 s counting time on the peak, using a beam diameter of 1 µm (for more details on the analytical procedures see Pitra et al., 2008). Mineral compositional variables and endmember proportions are based on molar proportions and expressed as follows: xMg = Mg/(Fe+Mg); for garnet, alm = Fe^{2+}/(Fe^{2+}+Mg+Ca+Mn), prp = Mg/(Fe^{2+}+Mg+Ca+Mn), grs = Ca/(Fe^{2+}+Mg+Ca+Mn), sps = Mn/(Fe^{2+}+Mg+Ca+Mn); for epidote, ep = Fe^{3+}/(Fe^{3+}+Al-2); for clinopyroxene, jd = Na/(Na+Ca); for white mica, xNa = Na/(Na+Ca+K); for plagioclase, ab = Na/(Na+Ca+K); for amphibole, structural formulae are calculated following Leake et al. (1997), Ca_B corresponds to the molar amount of Ca on the B (or M4) crystallographic sites. The sign "–" indicates a range in compositions, "→"a variation from core to rim, pfu = per formula unit.

Mineral abbreviations are as follows: garnet (g), muscovite (mu), paragonite (pa), undifferentiated clinopyroxene (cpx), omphacite (omp), clinoamphibole (am), epidote (ep), plagioclase (pl), biotite (bi), chlorite (chl), quartz (q), coesite (coe), rutile (ru), titanite (sphene, sph), lawsonite (law), kyanite (ky), zircon (zrc), carbonate (crb), apatite (ap) and symplectite (sym). Modes for the different major minerals were obtained by pixel counting on thin section-scale X-ray compositional maps for Na, Ca, Al, Mg and Mn.

3.2. Trace-element composition

Trace-element analyses of garnet and rutile were carried out at the GeOHeLiS analytical platform (OSUR, Univ. Rennes) by in-situ Laser Ablation Inductively Coupled Plasma Mass Spectrometry (LA-ICP-MS) using an ESI NWR193UC Excimer laser coupled with an Agilent quadrupole 7700x ICP-MS equipped with a dual pumping system for enhanced sensitivity (Paquette et al., 2014). For garnet, an ablation spot diameter of 80 µm with a repetition rate of 4 Hz and a fluence of 5.8 J·cm^{-2} was used. Major-element X-ray compositional maps were acquired on an electron microprobe prior to the trace-element analyses for the selected garnet grains to ensure accurate laser spot locations. Results were normalized to the NIST610 glass standard and SiO_2 content was used as internal standard, fixed at 38.3 wt % (for further information see Nosenzo et al., 2022). For rutile, ablation spot diameter of 50 µm with a repetition rate of 5 Hz and a fluence of 6.3 J·cm^{-2} were used. Results were normalized to the R10 rutile standard (Luvizotto et al., 2009). The R632 secondary rutile standard yielded Zr concentration of 4608±155 ppm, within error of the published value of 4294±196 ppm (Axelsson et al., 2018). Data reduction was carried out with the Iolite4 software (Paton et al., 2011). Detailed operating conditions for the trace-element analyses are available in Table S2.

3.3. Raman spectroscopy and quartz-in-garnet barometry

Raman spectra of quartz inclusions in several garnet grains were acquired on the University Rennes 1 Raman platform (SIR-ScanMAT). Analyses were carried out on a 30 µm-thick thin section and only rounded inclusions, maximum 20 µm wide, without any cracks and not in the vicinity of garnet fractures were analysed. A Horiba LabRAM HR800 micro-confocal spectrometer equipped with a 600 lines/mm grating was used with a 532 nm laser (laser power around 10 mW at the sample). With a x100 objective, lateral resolution (in the objective focal plane) was around 1 µm and axial resolution (along laser axis) was around 3 µm. Spectral range of -30–1700 cm^{-1} was recorded and spectral dispersion around 1.7 cm^{-1} was achieved. Synthetic quartz and pure silicon were used as standards and analysed throughout the session. Strain tensors of the quartz inclusions were calculated from the 128.1, 207.3 and 464.8 cm^{-1} Raman peak mode shifts using the stRAinMAN software (Angel et al., 2019). An uncertainty of 0.3 cm^{-1} was assumed for the shifts. Isomekes (i.e. lines in *P*–*T* space) of

possible quartz entrapment conditions were obtained using the EntraPT platform (Mazzucchelli et al., 2021) with either almandine, pyrope or grossular as host (equations of state for quartz from Angel et al., 2017; for garnet endmembers from Milani et al., 2015, 2017) and then recalculated with the measured garnet composition. The final propagated error issued from Raman shift uncertainties and misfit between the three modes results in pressure uncertainty of ± 0.3–1.5 kbar.

3.4. Phase-equilibrium modelling

Phase-equilibrium modelling was carried out in the MnNCKFMASHTO system ($MnO–Na_2O–CaO–K_2O–FeO–MgO–Al_2O_3–SiO_2–H_2O–TiO_2–Fe_2O_3$) using the Theriak/Domino software (de Capitani & Petrakakis, 2010) and the internally consistent thermodynamic dataset 6.2 (Holland & Powell, 2011). The following minerals and solution models were used: biotite, white mica, chlorite (White et al. 2014), amphibole and clinopyroxene (Green et al. 2016), epidote (Holland & Powell 2011), plagioclase (Holland & Powell 2003). Garnet *a–x* relations of White et al. (2007) were used instead of those of White et al. (2014) following the suggestions of Pan et al. (2020). Albite, lawsonite, quartz/coesite, rutile and titanite were considered as pure end-members. The analysed bulk rock composition was corrected for the presence of apatite and carbonates, not considered in the modelling, and the measured $X(Fe^{3+})$ ratio (molar Fe^{3+}/Fe^{total}) was used. Pure H_2O fluid was considered in excess. The presence of carbonates in the sample implies the presence of CO_2, which is known to shift the position of equilibria in the *P–T* field (e.g. Evans, 1990; Schumacher et al., 2008). However, several studies on carbonate-bearing HP rocks (Schumacher et al., 2008; Skelton et al., 2019; Manzotti et al., 2021) suggested very low $X(CO_2)$ in such systems (of the order of $X(CO_2)<0.03$), and consequently a limited impact on the modelled equilibria.

Thermobarometry for the symplectite assemblage was achieved with THERMOCALC 3.50 (Powell & Holland, 1988), using the average P calculation mode and the internally consistent thermodynamic dataset 6.2 (Holland & Powell, 2011).

4. Petrography and mineral chemistry

Eclogite sample NO7A was collected on Vågsøy island, ~50 metres from the Vågsberget museum (WGS84: 61.93106N, 5.05121E) from the core of an outcropping mafic lens (Figure 3a). The 3–4 metre-long lens is enclosed in a felsic migmatitic gneiss comprising quartz, plagioclase, garnet, biotite, epidote and amphibole. Towards the rim of the lens, eclogite progressively transitions to amphibolite.

The studied sample is a medium-grained well-preserved eclogite (Figure 3b, S1). It is composed of omphacite (55 %), garnet (30 %), white mica (8 %), epidote (1 %), green amphibole (1 %) and accessory kyanite, quartz, rutile, carbonates, zircon, apatite, ilmenite and magnetite. Elongation of

omphacite, white mica and epidote as well as garnet-rich layers define a foliation observable both macro- and microscopically.

Garnet is euhedral to subhedral, millimetre-sized and contains inclusions of quartz, epidote, amphibole, muscovite, titanite, rutile, omphacite, carbonates, ilmenite and zircon (Figure 3c–e). Garnet displays complex compositional zoning with three distinct zones named Grt I, Grt II and Grt III (Figure 3h-l, S2). Grt I shows rimward decreasing almandine and spessartine (alm = 0.55→0.46, sps = 0.06→0.01), increasing pyrope (prp = 0.12→0.22) and roughly constant grossular (grs = 0.30–0.32). X-ray compositional maps reveal locally irregular and patchy zoning in Mg (Figure 3i). Grt II is significantly richer in pyrope, which slightly increases rimwards (prp = 0.29→0.31), and significantly poorer in grossular, which slightly decreases (grs = 0.21→0.18). Almandine and spessartine are constant (alm = 0.49–0.51, sps = 0.01). Grt III has a homogeneous composition (alm = 0.46–0.49, sps = 0.01, prp = 0.27–0.28, grs = 0.22–0.24). Furthermore, the mineralogy of the included phases changes alongside garnet composition. Inclusions of quartz, epidote and scarce small titanite and rutile grains are mostly present in Grt I; amphibole, potassic white mica and carbonates in Grt I and II; omphacite and larger rutile grains (> 5 μm) in Grt I rim and Grt II; Grt III is almost inclusion-free apart from rutile and rare quartz and zircon. These three types of garnet are also characterized by specific REE distribution (Figure 4, S3). Grt I shows depletion in middle REE (MREE, Sm–Er) relative to Grt II and III, which are both richer in MREE and have similar scoop-shaped REE spectra. The three garnet zones lack or have weakly positive Eu anomalies, with Eu/Eu* = 0.99–2.17 for Grt I, 0.97–1.27 for Grt II and 1.13–1.37 for Grt III ($Eu/Eu^* = Eu_N/(Sm_N \cdot Gd_N)^{0.5}$). Garnet inclusions in clinopyroxene and white mica are chemically similar to Grt I and Grt II (alm = 0.45–0.50, grs = 0.31→0.23, prp = 0.20→0.28, sps = 0.02→0.01).

Clinopyroxene is millimetre-sized (Figure 3b), subhedral, and contains inclusions of garnet, white mica, quartz, rutile, amphibole, zircon and rare kyanite (Figure 3g). Clinopyroxene crystals found in the matrix or included in garnet have a composition of omphacite and are slightly zoned (jd = 0.56→0.50, Al = 0.53→0.49 pfu, recalculated Fe^{3+} = 0.00–0.05 pfu; Figure S4). In the vicinity of fractures, clinopyroxene is surrounded and progressively replaced by a very fine-grained symplectite comprising less-jadeitic clinopyroxene (50 vol.%; jd = 0.25–0.29, Al = 0.27–0.36 pfu), plagioclase (40 vol.%; ab = 0.84–0.88) and amphibole (10 vol.%; edenite with Si = 6.50–6.71 pfu, xMg = 0.68–0.74, Ca_B = 1.83–2.00).

Potassic (phengitic) white mica is present in the sample as millimetre-sized matrix grains. It contains garnet, rutile and zircon inclusions. It is weakly zoned with rimward decreasing Si = 3.40→3.25 pfu and increasing xNa = 0.14→0.21 (Figure S5). White mica crystals included in clinopyroxene have the

same range of compositions. Inclusions in garnet show increasing Si content from garnet core to rim (Si = 3.24 pfu in Grt I, 3.27–3.37 pfu in Grt II). The sample also contains paragonite (xNa = 0.89–0.92), which locally overgrows muscovite and whose elongation is mostly oblique to the general foliation of the sample (Figure 3b).

Epidote is rare and significantly less ferric in the matrix (ep = 0.12–0.19) than the inclusions in garnet or clinopyroxene (ep = 0.35–0.40). Amphibole shows variable composition depending on the textural position in the sample. Rare matrix grains consist of green to slightly blue amphibole with inclusions of quartz, epidote and garnet and have Si = 6.62–6.75 pfu, xMg = 0.72–0.76, Ca_B = 1.21–1.27. A thin corona (10–15 µm large) of green amphibole (Si = 5.64–6.46 pfu, xMg = 0.52–0.71, Ca_B = 1.31–1.86) is commonly present around garnet. Amphibole included in garnet shows variable composition with Si = 5.53–6.13 pfu, xMg = 0.40–0.69, Ca_B = 1.36–1.56. Carbonate minerals are present in small quantities (<1 %) throughout the sample and are found both in the matrix or as inclusions in the major mineral phases. They are mostly dolomite, although an inclusion of calcite has been observed in an omphacite grain. Rutile analyses on 42 grains yield variable zirconium contents between 66 and 158 ppm. One rutile grain was discarded from the thermometry calculations because of its anomalous Zr concentration of 443 ppm, possibly caused by the presence of Zr-rich micro-inclusions (see Section 5.3 below; Table S6). The inferred paragenetic sequence is summarised in Figure 5. Representative microprobe analyses (Table S3) and detailed trace-element analyses of garnet (Table S5) are available in the Supplements.

5. *P–T* estimates

5.1. Phase-equilibrium modelling

In the *P–T* pseudosection (Figure 6a), garnet, clinopyroxene and amphibole are stable throughout the *P–T* range considered, except for the loss of amphibole in the HP–HT corner. Biotite and muscovite are stable at pressures respectively lower and higher than ~10 kbar in the temperature range considered. Biotite is also stable in the HP–LT corner of the diagram, whereas muscovite is absent. Rutile is replaced by titanite at pressures lower than 14–15 kbar. Quartz is stable in the LP–HT part (T > 500 °C at 10 kbar and P < 21 kbar at 700 °C) and in the HP–HT corner of the diagram. Kyanite is present above 20 kbar at temperatures higher than 620 °C. Epidote is stable below 17 kbar at 500 °C and below 23 kbar at 620 °C. The earliest assemblage inferred from inclusions in Grt I (quartz, epidote, amphibole, muscovite, titanite) is stable at 510–650 °C and 11–14 kbar. Considering the rare tiny inclusions of rutile, this field can be extended towards higher pressure, as the incorporation of Al (not considered in the modelling) may stabilise titanite towards higher pressures (Carswell et al., 1996; Troitzsch & Ellis, 2002). The composition of Grt I core (grs = 0.30–0.32, prp =

0.12) points to crystallisation at either 22 kbar–550°C or 17 kbar–600°C (Figure 6b). However, only the latter set of conditions is compatible with the inclusion assemblage, in particular the presence of quartz and epidote, and the spessartine content of Grt I core (sps = 0.06; Figure 6d). The composition of Grt I rim (grs = 0.30, prp = 0.22, sps = 0.01) suggests equilibration at ~23 kbar–600 °C, at the lawsonite-epidote transition. The composition of Grt II (grs = 0.18–0.20, prp = 0.28–0.30) and the maximal Si content in phengite (Si = 3.40 pfu) correspond to peak-pressure conditions of 600 °C and 27–29 kbar (Figure 6b–c). The composition of Grt III (grs = 0.22–0.24, prp = 0.28), inclusions of kyanite in omphacite and the presence of scarce quartz both in the matrix (Figure 3b) and included in Grt III imply heating to 660–680 °C. The absence of coesite suggests no pressure increase. Finally, amphibole coronae around garnet, plagioclase-bearing symplectites around omphacite and paragonite overgrowing phengite record the subsequent decompression. These decompression textures are present only in some microdomains of the sample and testify to local equilibration, limiting the use of phase-equilibrium modelling to constrain the *P*–*T* conditions that prevailed.

5.2. Quartz-in-garnet barometry

Quartz-in-garnet (QuiG) barometry performed on 32 inclusions found in 11 different garnet grains yields entrapment pressures of 5–15 kbar at 500 °C and 9–18 kbar at 700 °C (Figure 7). As all the analysed quartz inclusions are located in Grt I, the uncertainty in the calculated pressures stemming from the variable composition of the surrounding host garnet was bracketed by using alternatively Grt I core and Grt I rim compositions as host. The two garnet compositions result in entrapment pressures within 0.1 kbar of each other, which is negligible when taking into account the analytical uncertainty (±0.3–1.5 kbar). A single representative garnet composition was therefore used for all inclusions (alm = 0.55, grs = 0.30, prp = 0.15).

For a given temperature, quartz inclusions in each individual garnet grain yield entrapment pressures within a 2.5 kbar range except for garnet grain 13 whose inclusions yield entrapment pressures between 8.1 and 12.7 kbar (Table S7). With entrapment pressures below 10 kbar limited to two garnet grains (garnet 1 and 19, Table S7), most of the isomekes lie within a 12–15.2 kbar range at 600 °C.

5.3. Trace- and major-element thermobarometry

Zr-in-rutile thermometry was performed in order to bring additional constraints on the temperature reached by this eclogite sample. The calibration of Ferry & Watson (2007) yields an average temperature of 564±17 °C with $a(SiO_2)$ assumed at unity, in agreement with the presence of inclusions of quartz together with rutile and zircon in omphacite (Figure 3f). The pressure-dependent calibration for α-quartz from Tomkins et al. (2007) gives temperatures of 590±18 °C at 15 kbar and

630±18 °C at 25 kbar (Figure 8). In both cases, the errors on the measurement of the Zr concentration result in a maximum uncertainty of ±2 °C, which is negligible compared to the uncertainties inherent to the calibrations themselves, i.e. ±40 °C for Ferry & Watson (2007), ±30 °C for Tomkins et al. (2007). Given the (U)HP conditions reached by the sample, the effect of pressure on the thermometer is probably significant. The results obtained with the pressure-dependent calibration of Tomkins et al. (2007) are thus preferred (Figure 8).

For the symplectite, the plagioclase–amphibole thermometer for quartz-free assemblages of Holland & Blundy (1994) yields temperatures of 591±9 °C at 5 kbar and 675±8 °C at 15 kbar (Figure 8). Clinopyroxene-amphibole-plagioclase thermobarometry achieved through the average P calculation mode with THERMOCALC yields pressures of 10.0±1.5 kbar at 500 °C and 12.7±1.4 kbar at 700 °C (Figure 8; Table S4).

6. Discussion

6.1. Metamorphic evolution

From all the above results, a *P–T* evolution is proposed in Figure 8. Overall, there is a good agreement between the QuiG barometry results and the modelled stability field of the inclusion assemblage in Grt I core (i.e., q-ep-am-mu-sph±ru) at 510–650 °C and 11–15 kbar, just above the plagioclase-out line (Figure 6a). The rounded shape of many of the included crystals of quartz and epidote and their location away from fractures (e.g. Figure 3c,d) testify to their primary, prograde character (rather than their formation during the retrograde evolution). The irregular shape of some of the inclusions of epidote is compatible with the modelled decrease of the proportion of epidote along the inferred *P–T* path and consequently its partial resorption during the crystallisation of garnet. Nevertheless, the pressure inferred from the intersection of the composition isopleths for the crystallisation of the Grt I core (17 kbar), is about 2 kbar higher than the maximum QuiG pressure (~15 kbar). Furthermore, the spread of the QuiG results towards low pressure (garnet grains 11, 13 and 19, Table S7) could question the reliability of this method. However, Bonazzi et al. (2019) suggested that partially exposed grains may have lost stress, yielding entrapment pressures up to 8 kbar lower than for fully enclosed quartz inclusions. This apparent drop in pressure could correspond to the discrepancy observed between the few low values when compared to the bulk of the results (Figure 7). The spread of QuiG pressure estimates may also reflect later mechanical modifications, such as brittle or plastic deformation of the inclusion-host interface (Thomas & Spear, 2018) or that some of the analysed quartz inclusions are too close to the thin-section surface (Campomenosi et al., 2018). On the other hand, to the best of our knowledge, post-entrapment processes that could lead to an artificial pressure increase have not yet been proposed. Therefore,

QuiG barometry may reflect underestimated but not overestimated entrapment conditions. In the present case, the data are compatible with the crystallisation conditions of the Grt I core and with the inferred prograde *P–T* path. Although our data bring no strong constraints on the temperature of the pre-garnet *P–T* conditions, the Grt I core composition points to a crystallization temperature at 600 °C that represents an upper limit. Our estimation for the pre-eclogite-facies metamorphic stage (510–600 °C, 11–16 kbar) lies at a slightly higher pressure than the Barrovian metamorphism (560–700 °C, 8–13 kbar) suggested by Hacker et al. (2010) and mostly observed in the nappes overlying the WGC (Hacker & Gans, 2005). The lack of metamorphic record older than the inclusions in garnet prevents extension of the *P–T* path to lower pressures.

Garnet zoning records an increase in pressure from 16 kbar to the peak pressure at 28–29 kbar, supported by the Si content in phengite. The rapid decrease in the grossular content (Figure 3g) between Grt I and Grt II corresponds to the transition between the epidote and the lawsonite stability fields at 23 kbar (Figure 6b). This is compatible with the presence of epidote inclusions exclusively in Grt I and supported by the REE spectra of the different garnet zones (Figure 4). Depletion of MREE in Grt I is attributed to the concomitant stability of epidote, which is the main light to middle REE host (Spandler et al., 2003). As soon as the rock leaves the epidote stability field during the prograde path, epidote breakdown makes MREE available again, explaining the enrichment in MREE in Grt II and Grt III relative to Grt I. Konrad-Schmolke et al. (2008) interpreted similarly the rimward evolution of the REE composition in some eclogitic garnets from the WGR. Their combined thermodynamic and REE-composition modelling also suggests that a decreasing mode of amphibole, evidenced in our sample by the scarcity of amphibole in the matrix compared to its more common presence as inclusions in garnet, may also explain such an enrichment. Moreover, Spandler et al. (2003) suggested that breakdown of titanite, which also hosts significant MREE, to form REE-poor rutile during prograde metamorphism may also contribute to the relative enrichment in MREE in the newly grown garnet.

The inferred prograde *P–T* path could be questioned with respect to the presumption of H_2O saturation and the possibility of garnet growth in the lawsonite stability field, due to the strongly hydrated character of lawsonite and the subsequent possible fluid undersaturation (e.g. Ballèvre et al., 2003; Clarke et al., 2006; López-Carmona et al., 2013). Indeed, the inferred *P–T* evolution from Grt I core to Grt I rim is associated with progressive dehydration, associated with the progressive loss of epidote. At the conditions inferred for the growth of Grt I rim (600 °C, 23 kbar), 2.83 mol% of H_2O are necessary to saturate the mineral assemblage, while the assemblage at 600 °C, 28 kbar (Grt II) requires 6.1 mol% of H_2O. Strictly speaking, this implies additional hydration during compression. However, 6.1 mol% of H_2O at 600 °C, 23 kbar only produces 2.6 volume % of free fluid. This amount

is well in the range estimated for the amount of fluid possibly present in the deep lithosphere (Thompson & Connolly, 1990). Furthermore, Angiboust & Raimondo (2022) reported the possible presence under eclogite-facies conditions of significant porosities, which could be up to 4 volume %. Phase-equilibrium modelling under H_2O saturation thus still appears as a valid approach in this case. Finally, the shape of the isopleths of spessartine (Figure 6d, S6d), which are (sub)parallel to those of garnet mode, testify to the possibility of garnet growth during compression and/or heating.

Given the mode of garnet and its strong chemical zoning, compositional fractionation should be taken into account when modelling phase equilibria. However, modelling at constant effective bulk composition (Figure 6) on the one hand and with fractionation of garnet cores on the other hand resulted in very similar *P*–*T* diagrams (Figures S6 & S7). With respect to Figure 6, garnet fractionation results in the displacement of the garnet-in line towards higher temperatures, but the general topology as well as the position of the compositional isopleths are affected only marginally. For more accuracy, fractionation of omphacite was also taken into account when evaluating the effective bulk composition used to model Grt III growth (Figure S7). Again, this diagram confirms the results obtained using the unfractionated bulk composition and the inferred *P*–*T* path. Finally, results from the Zr-in-rutile thermometry using the pressure-dependent calibration of Tomkins et al. (2007) are compatible with rutile growth during heating (Figure 8). These results overlap the *P*–*T* conditions inferred for Grt III growth in the quartz and kyanite stability field at 660–680 °C and 27–28 kbar, limited towards higher pressures by the absence of coesite or polycrystalline quartz. The inferred temperature range for the eclogite-facies metamorphism agrees with the estimates from nearby eclogites of 645±50 °C and 729±80 °C of Labrousse et al. (2004) and Krogh Ravna & Terry (2004), respectively. However, while the latter found pressures of 29±3 kbar, in agreement with our estimates, Labrousse et al. (2004) obtained lower pressures of 21.5±2.5 kbar using the THERMOCALC average PT method.

In our sample, the decompression is only recorded by the symplectites. The *P*–*T* range inferred from the clinopyroxene-amphibole-plagioclase and plagioclase-amphibole equilibria (Figure 8) implies nearly isothermal decompression from 27–28 kbar down to 10–14 kbar at 620–680 °C. These results point to slightly higher *P*–*T* conditions than the estimations of Labrousse et al. (2004) for symplectites in another eclogite from Vågsvåg (550–620 °C, 8.7–12.6 kbar), conditions that can be applied more broadly to the whole Nordfjord area (Labrousse et al., 2004; Young et al., 2007; Figure 2). They are consistent with the *P*–*T* conditions inferred for symplectites from the Stadlandet peninsula by Carter et al. (2021) for the point from which isothermal decompression was succeeded by cooling (10–15 kbar, 650–700 °C). It is however difficult to determine in our sample whether or not the nearly isothermal decompression continued to lower pressures before cooling (Figure 2).

To the best of our knowledge, this is the first evidence of an isothermal compression for a crustal mafic body in the Western Gneiss Region. Such an isothermal prograde evolution has been described by Bhowany et al. (2018) on the Holsnøy island in the Bergen Arcs, south of the study area, where granulites preserve the transformation to hydrous eclogite from 680 °C–15 kbar to peak conditions of 680 °C–22 kbar and their subsequent retrogression to 690 °C–17 kbar. Nearly isothermal compression has also been recognized in other (U)HP terranes, such as in the Kokchetav massif in Kazakhstan (Masago, 2000; Stepanov et al., 2016) or the Chinese Su-Lu province (Enami et al., 1993). Such a metamorphic evolution is rather rare, but not unique, and tectonic contexts that could explain such *P–T* paths therefore deserve to be discussed.

6.2 Polycyclic scenario

The above conclusions only hold, however, if the different metamorphic stages belong to the same orogenic cycle. Indeed, both Sveconorwegian (e.g. Krabbendam et al., 2000; Wain et al., 2001; Corfu et al., 2014) and early Caledonian (e.g. Klonowska et al., 2016) metamorphic events have been reported in the Caledonides. It could be consequently considered that in the studied sample, Grt I is a relic from an earlier metamorphic cycle. For instance, in-situ Lu–Hf dating of garnet in a felsic gneiss from Verpeneset (Figure 1b) revealed a 913±63 Ma age in the core while the rim yielded a Scandian age of 405±25 Ma (Tamblyn et al., 2021). Sveconorwegian rocks are relatively common in the study area, as for instance in the Flatraket, Ulvesund and Kråkeneset localities (Figure 1b). However, they exclusively record amphibolite to granulite-facies conditions with pressures around 10 kbar (Wain et al., 2001; Faryad et al., 2022). In the studied sample, Grt I displays a continuous core-to-rim chemical zoning that implies, given the results of the phase-equilibrium modelling, isothermal compression at 600 °C from 17 kbar to 23–24 kbar, in the eclogite facies, whatever its age. Accordingly, garnet included in omphacite is in textural equilibrium with omphacite, is chemically similar to Grt I rim, and is thus an eclogite-facies phase. Such conditions have not been described in the Sveconorwegian rocks and conflict with the published records.

Alternatively, an early Caledonian, pre-Scandian, HP metamorphism of Ordovician age has been revealed by numerous geochronological studies in the allochthons and a polycyclic, multiple subduction-eduction model (“dunk tectonics”) has been proposed for the evolution of the Scandinavian Caledonides (e.g. Brueckner & Roermund, 2004; Majka et al., 2014; Walczak et al., 2019). However, geochronological data available for the basement in this part of the WGR (roughly the spatial extent of the map in Figure 1b) rather report unequivocally Scandian ages. Few older ages, ranging between 430 and 500 Ma, are undistinguishable from the Scandian phase because of their large

uncertainties (e.g. Griffin & Brueckner, 1985; Tamblyn et al., 2021). It appears that the pre-Scandian phase of the Caledonian Orogeny is not recorded within the WGC basement (March et al., 2022).

Finally, and most importantly, the continuity of the chemical zoning suggests that the growth of Grt II continuously followed Grt I growth. This is best seen in the detailed compositional profiles (Figure S2). Furthermore, polymetamorphic garnets typically display textural and chemical features typical of garnet resorption such as jagged grain boundaries, fractures, annuli of increased spessartine content, annuli of concentrated inclusions (e.g. Le Bayon et al., 2006; Feenstra et al., 2007; Zulbati, 2011; Manzotti & Ballèvre, 2013). Such features are not observed in the rock. Although the absence of evidence is not evidence of absence, these observations do not support a polycyclic interpretation of the studied sample.

Although some localized features in the compositional maps (Figure 3h–j) may be *interpreted* as garnet dissolution, they are exclusively present between Grt II and Grt III. Furthermore, the compositional maps, for Ca especially, highlight that such a phenomenon is only local and not a general feature for garnet. It could be argued that dissolution related to sample-scale phenomena (such as changing *P–T* conditions) should be visible on all garnet faces. Other explanations, such as garnet growth against another grain dissolved before Grt III growth, could be proposed without any easy solution to discriminate between the different hypotheses. Finally, even taking into account some partial dissolution of garnet before the growth of Grt III, would not change the first-order *P–T* path inferred for our sample.

6.3. Geodynamic implications

Rocks metamorphosed in subduction zones are thought to commonly undergo a rapid increase of pressure, accompanied by an increase of temperature, albeit only limited (typically in the order of 8 °C.km^{-1}, e.g. Miyashiro, 1972; Ernst, 2001; Penniston-Dorland et al., 2015; Agard et al., 2022). However, the apparent absence of a temperature increase during compression for our sample seems incompatible with this classic view and may question the tectonic significance of (U)HP metamorphism. In the recent literature, the true meaning of the pressure estimates remains highly debated (e.g. Schmalholz & Podladchikov, 2013; Moulas et al., 2014; Gerya, 2015; Yamato & Brun, 2017; Luisier et al., 2019; Bauville & Yamato, 2021; Tajčmanová et al., 2015, 2021), as pressure may not be always purely lithostatic (that is, proportional to depth). Depending on how pressure estimates are interpreted, the models of tectonic reconstruction can highly differ. In that sense, the interpretation of the isothermal compression we obtained deserves to be discussed. Two end-member geodynamic scenarios can be then considered:

In the first scenario, it is considered that the pressure is purely lithostatic. In this case, the only way to explain an isothermal compression is to bury the rocks without any temperature variation. A simple explanation for this process would be to consider rapid burial, such that heating does not occur (i.e., thermal advection faster than diffusion). For instance, Jamtveit (1987) suggested that rapid crustal thickening by stacking during continental collision could explain the near-isothermal compression from 5 kbar to more than 25 kbar of an eclogite from Eiksunddal (Figure 1b). However, this conflicts with the findings of Kylander-Clark et al. (2009), who inferred slow subduction (with vertical burial rate of 2–4 $mm.y^{-1}$) for the WGR from combined garnet dating and numerical modelling. Cutts & Smit (2018) obtained a similar burial rate (~5 $mm.y^{-1}$), also by garnet dating. Alternatively, thermal modelling of continental subduction zones and collisions (e.g. Faccenda et al., 2009; Fauconnier et al., 2014) shows that isothermal burial is possible away from the subduction interface, considering deeper level of the lower plate. Fauconnier et al. (2014) showed by numerical modelling that the lower continental crust and the underlying mantle of the down-going slab remain thermally undisturbed up to depths of almost 100 km (Figure 9a). Kylander-Clark et al. (2009) obtained a very similar thermal state while modelling the *P*–*T*–*t* history of the WGR when considering that the WGR has derived from a thick crustal section. Therefore, bodies embedded in such a lower crust could be buried parallel to the 600 °C isotherm (Figure 9a), resulting in an isothermal compression (Figure 9b). On the other hand, isothermal compression would be impossible or very limited for rocks initially at shallower depths and lower temperatures (blue arrow in Figure 9a–b). This implies that the studied mafic body must be derived from the middle to lower crust of a thick crustal section and already at 600 °C at the onset of burial. However, a shallower crustal origin for the bedrock and its mafic lenses seems possible when taking into account a more complex stratigraphy of the subducting slab. For instance, Young (2018) suggested that the study area comprised delaminated parts of the upper Baltica crust. Moreover, based on U–Pb dating of intrusive rocks, Jakob et al. (2017) and Andersen et al. (2022) suggested that the Baltica margin experienced extension from the Late Cambrian until the Middle Ordovician. In such a context, lithospheric thinning (and related exhumation of the mantle) would have caused a temperature increase of the crust (including the mafic lenses), potentially up to 600 °C. In this case, the stacking of the allochthons from the hyperextended margin would result in compression during the first stages of shortening, perhaps up to the inferred amphibolite-facies pressure conditions. As for an originally thick crust, subsequent isothermal burial would be possible for the base of the crust. After reaching the maximum burial, the rocks were heated by thermal diffusion from the hot mantle wedge. This may explain the temperature increase between the growth of Grt II (i.e., peak pressure) and Grt III in our sample. Stepped *P*–*T* paths (i.e., alternating between pressure increase at constant

temperature, and temperature increase at constant pressure) along very low thermal gradient are predicted by some geodynamic models of continental (Li et al., 2010) and oceanic subduction (Syracuse et al., 2010). In the Kokchetav Massif, Stepanov et al. (2016) related to such models the *P*–*T* path of a kyanite-bearing mica-schist, showing a pressure increase from 11 to 23 kbar at 500–550 °C, followed by heating to peak conditions at 700 °C, 24 kbar. Almost isobaric heating is attributed to the coupling of the subducted slab with the hanging wall mantle.

The second scenario takes into account the possibility that part of the recorded pressure is tectonic in origin. Here, during the first stage of prograde evolution, not recorded in our sample, the increase of both temperature and pressure could be attributed to the burial of rocks across the isotherms during subduction (Figure 9c) up to the amphibolite-facies *P*–*T* conditions (Figure 9e). Introduction of low-density continental crust into a denser mantle perturbs the subduction dynamics. Due to the positive buoyancy of the continental crust, coupling occurs between the overriding and subducting plates during the collisional stage of the orogeny (Figure 9d), with a necessary increase of horizontal stress. This mechanically leads to an increase of the deviatoric stress sustained by the rocks (Figure 9d inset) and therefore to a pressure increase (Petrini & Podladchikov, 2000; Mancktelow, 2008; Yamato & Brun, 2017). Reuber et al. (2016) showed that strong lower crust or strong heterogeneities therein may be indeed subject to large (> +100 %) deviations from lithostatic pressure during collision. Based on a wide dataset of metamorphic records from various (U)HP terranes, Yamato & Brun (2017) suggested that the peak pressure recorded in (U)HP rocks and the subsequent pressure drop were linearly related and could be explained by a switch of the state of stress between compression (burial) and extension (exhumation). Their mechanical analysis considered pressure-dependent frictional yielding, i.e. brittle behaviour depending linearly on pressure through the friction angle and the cohesion of rocks, which are chosen to follow Byerlee's law. Considering a friction angle of 30° and neglecting cohesion of rocks, they inferred that the peak pressure P_c and the lithostatic pressure P_{litho} were related so that $P_c = 2 \cdot P_{litho}$, which is in agreement with our data. Indeed, when considering that the prograde amphibolite-facies pressure (~14 kbar) reflects the maximal lithostatic pressure, the peak pressure inferred from garnet and phengite (~28 kbar) follows this simple relation. As thermal equilibration in the orogenic root is limited before the slab break-off, this compression may occur isothermally. In the WGR, thermal insulation from the mantle wedge provided by the allochthon blanket, as proposed by Hacker et al. (2010), may also help explaining (near) isothermal processes. At the onset of exhumation (that is, the switch between compression and extension), slab break-off occurs as proposed in the eduction model for the Norwegian Caledonides (e.g. Andersen & Jamtveit, 1990; Andersen et al., 1991; Dewey et al., 1993), explaining the temperature increase at peak pressure by thermal equilibration (e.g. Warren, 2013). In the

model of Yamato & Brun (2017), this switch from compression to extension leads to a pressure drop such that the recorded pressure in extension P_e follows the relation $P_e = ⅔ \cdot P_{litho}$ (considering a friction angle of 30° and neglecting cohesion as above). Our data are also compatible with this model as the pressure range inferred for the symplectite formation (~10–14 kbar) overlaps the interval that corresponds to two thirds of the pressure range inferred for the prograde amphibolite-facies.

Alternatively, on the Holsnøy island in the Bergen Arcs, where Bhowany et al. (2018) suggested an isothermal prograde evolution for an eclogite, Jamtveit et al. (2018) attributed the eclogite-facies metamorphism to a local weakening of some rock volumes in a highly stressed and dry lower crust due to fluid infiltration. Their modelling shows that the weak eclogite contained in strong granulite may have experienced overpressure up to 5 kbar, explaining the pressure gap between the inferred amphibolite-facies conditions of ~15 kbar that are assumed to reflect the lithostatic pressure, and the peak-pressure, eclogite-facies conditions. However, the explanation proposed by Jamtveit et al. (2018) may probably not be applied to our eclogite body. On Holsnøy, eclogite-facies rocks are found in originally rather dry (and strong) homogeneous granulites. This situation is largely different from the majority of the eclogites in the WGR, where they occur as lenses and pods within the Western Gneiss Complex.

Finally, the ~14 kbar compression inferred in our sample between the amphibolite facies and the peak pressure does not need to reflect pure tectonic pressure; compression with both lithostatic and tectonic pressure components is possible, although evaluating the contribution of each component seems arduous (Bauville & Yamato, 2021).

We emphasize, however, that the *P*–*T* evolution proposed here and the subsequent interpretation of the isothermal compression as a possible marker of tectonic pressure is based solely on one eclogite sample. Other eclogites in the Nordfjord-Stadlandet area may have experienced different fates: (1) The occurrence of melting at peak-pressure conditions, which is still debated in the WGR (Labrousse et al., 2011; Ganzhorn et al., 2014), may largely influence the rheology and the pressure experienced by the eclogites: finite-element modelling of an eclogite lens within a pod of partially melted gneiss confined in unmelted gneiss showed that pressure experienced by the eclogite can deviate from purely lithostatic by up to +30–40 kbar (Vrijmoed et al., 2009). (2) Magnitude of overpressure experienced by a volume of rocks is largely dependent on its shape and orientation relative to the principal stresses direction (Vrijmoed et al., 2009; Moulas et al., 2014; Cutts et al., 2020), parameters that could indeed be different from one eclogite occurrence to another in the Nordfjord-Stadlandet region (Hacker et al., 2010). All of this would argue for local rather than kilometre- to regional-scale processes, and may conflict with the apparent coherence of the

metamorphic peak pressure gradient seen in the Nordfjord-Stadlandet zone and more broadly in the whole WGR. In that sense, the fact that the peak pressure inferred for the studied eclogite fits well in the regional pressure gradient (Figure 1b) could be an argument against tectonic overpressure, excepted when considering that the rocks experienced the same percentage of tectonic overpressure.

We acknowledge that our results, although well-constrained, do not permit to propose conclusive geodynamic implications. It is noteworthy that the two geodynamic scenarios proposed are not necessarily incompatible. A mafic lens embedded at depth (~40–50 km) in the lower crust could be buried isothermally at temperature conditions around 600 °C before experiencing overpressure. Although the important post-UHP amphibolite overprint recognized in the whole WGR is an obstacle to the comprehension of pre-UHP tectonics, more detailed studies like this one are necessary to get a better understanding and quantification of the early stages of the Caledonian subduction.

7. Conclusions

Detailed petrological analysis revealed a significant part of the *P–T* path for a mafic eclogite from the Nordfjord-Stadlandet zone. Prograde evolution is characterized by an isothermal compression at 600 °C from pressures of 11–16 kbar (amphibolite-facies conditions) to 27–29 kbar (eclogite-facies conditions), followed by a near-isobaric heating to 660–680 °C. Retrogression then occurred during nearly isothermal decompression to 10–14 kbar and 620–680 °C. While isothermal decompression has been largely described in the Western Gneiss Region, the isothermal compression highlighted here provides new data to constrain the tectonic evolution of the WGR. Such isothermal pressure increase remains however difficult to interpret. We propose that this could be due either to a deep burial (100 km) of a thermally undisturbed lower-crust material or to up to 14 kbar of tectonic overpressure occurring during collision.

Acknowledgements

This research was supported by a Rennes 1 University grant to P. Pitra (Défis Scientifiques program) and by the GeOHeLiS platform. P. Yamato thanks the Institut Universitaire de France for financial support. We are very grateful to Xavier Le Coz for thin section preparation and Jessica Langlade for her help during the mineral microprobe analyses. Alain Moréac, Katy Leroy and Alexandre Peillod are thanked for the analytical support for the Raman spectroscopy, the data acquisition, and useful suggestions on data treatment, respectively. This study is a part of the PhD thesis of M. Simon, funded by the French Ministry of Higher Education and Research. The authors also thank C. Möller, J. Majka and two anonymous reviewers who helped to improve the quality of this contribution.

References

Agard, P., Soret, M., Bonnet, G., Ninkabou, D., Plunder, A., Prigent, C., & Yamato, P. (2022). Subduction and obduction processes : The fate of oceanic lithosphere revealed by blueschists, eclogites and ophiolites. In *Compressional Tectonics : Plate Convergence to Mountain Building—Volume 2* (Catlos; Cehmen; Dalziel (Eds.)). American Geophysical Union. https://doi.org/10.1002/essoar.10510507.1

Andersen, T. B. (1998). Extensional tectonics in the Caledonides of southern Norway, an overview. *Tectonophysics*, *285*(3-4), 333-351. https://doi.org/10.1016/S0040-1951(97)00277-1

Andersen, T. B., Jakob, J., Kjøll, H. J., & Tegner, C. (2022). Vestiges of the Pre-Caledonian Passive Margin of Baltica in the Scandinavian Caledonides : Overview, Revisions and Control on the Structure of the Mountain Belt. *Geosciences*, *12*(2), 57. https://doi.org/10.3390/geosciences12020057

Andersen, T. B., & Jamtveit, B. (1990). Uplift of deep crust during orogenic extensional collapse : A model based on field studies in the Sogn-Sunnfjord Region of western Norway. *Tectonics*, *9*(5), 1097-1111. https://doi.org/10.1029/TC009i005p01097

Andersen, T. B., Jamtveit, B., Dewey, J. F., & Swensson, E. (1991). Subduction and eduction of continental crust : Major mechanisms during continent-continent collision and orogenic extensional collapse, a model based on the south Norwegian Caledonides. *Terra Nova*, *3*(3), 303-310. https://doi.org/10.1111/j.1365-3121.1991.tb00148.x

Anderson, E. D., & Moecher, D. P. (2007). Omphacite breakdown reactions and relation to eclogite exhumation rates. *Contributions to Mineralogy and Petrology*, *154*(3), 253-277. https://doi.org/10.1007/s00410-007-0192-x

Angel, R. J., Alvaro, M., Miletich, R., & Nestola, F. (2017). A simple and generalised P–T–V EoS for continuous phase transitions, implemented in EosFit and applied to quartz. *Contributions to Mineralogy and Petrology*, *172*(29), 15. https://doi.org/10.1007/s00410-017-1349-x

Angel, R. J., Murri, M., Mihailova, B., & Alvaro, M. (2019). Stress, strain and Raman shifts. *Zeitschrift Für Kristallographie - Crystalline Materials*, *234*(2), 129-140. https://doi.org/10.1515/zkri-2018-2112

Angiboust, S., & Raimondo, T. (2022). Permeability of subducted oceanic crust revealed by eclogite-facies vugs. *Geology*, *50*(8), 964-968. https://doi.org/10.1130/G50066.1

Austrheim, H. (1987). Eclogitization of lower crustal granulites by fluid migration through shear zones. *Earth and Planetary Science Letters*, *81*(2-3), 221-232. https://doi.org/10.1016/0012-821X(87)90158-0

Axelsson, E., Pape, J., Berndt, J., Corfu, F., Mezger, K., & Raith, M. M. (2018). Rutile R632—A New Natural Reference Material for U-Pb and Zr Determination. *Geostandards and Geoanalytical Research*, *42*(3), 319-338. https://doi.org/10.1111/ggr.12213

Ballèvre, M., Pitra, P., & Bohn, M. (2003). Lawsonite growth in the epidote blueschists from the Ile de Groix (Armorican Massif, France) : A potential geobarometer. *Journal of Metamorphic Geology*, *21*(7), 723-735. https://doi.org/10.1046/j.1525-1314.2003.00474.x

Bauville, A., & Yamato, P. (2021). Pressure-to-Depth Conversion Models for Metamorphic Rocks : Derivation and Applications. *Geochemistry, Geophysics, Geosystems*, *22*(1), e2020GC009280. https://doi.org/10.1029/2020GC009280

Beckman, V., Möller, C., Söderlund, U., Corfu, F., Pallon, J., & Chamberlain, K. R. (2014). Metamorphic zircon formation at the transition from gabbro to eclogite in Trollheimen–Surnadalen, Norwegian Caledonides. *Geological Society, London, Special Publications*, *390*(1), 403-424. https://doi.org/10.1144/SP390.26

Bhowany, K., Hand, M., Clark, C., Kelsey, D. E., Reddy, S. M., Pearce, M. A., Tucker, N. M., & Morrissey, L. J. (2018). Phase equilibria modelling constraints on P–T conditions during fluid catalysed conversion of granulite to eclogite in the Bergen Arcs, Norway. *Journal of Metamorphic Geology*, *36*(3), 315-342. https://doi.org/10.1111/jmg.12294

Bingen, B., Nordgulen, Ø., & Viola, G. (2008). A four-phase model for the Sveconorwegian orogeny, SW Scandinavia. *Norwegian Journal of Geology*, *88*, 43-72.

Bonazzi, M., Tumiati, S., Thomas, J. B., Angel, R. J., & Alvaro, M. (2019). Assessment of the reliability of elastic geobarometry with quartz inclusions. *Lithos*, *350-351*, 105201. https://doi.org/10.1016/j.lithos.2019.105201

Brueckner, H. K. (2018). The great eclogite debate of the Western Gneiss Region, Norwegian Caledonides : The in situ crustal v. exotic mantle origin controversy. *Journal of Metamorphic Geology*, *36*(5), 517-527. https://doi.org/10.1111/jmg.12314

Brueckner, H. K., & Roermund, H. L. M. van. (2004). Dunk tectonics : A multiple subduction/eduction model for the evolution of the Scandinavian Caledonides. *Tectonics*, *23*(2). https://doi.org/10.1029/2003TC001502

Bryhni, I. (1966). Reconnaissance Studies of Gneisses, Ultrabasites, Eclogites and Anorthosites in Outer Nordfjord, Western Norway. *Norges Geologiske Undersøkelse*, *241*, 68.

Bryhni, I., & Griffin, W. L. (1971). Zoning in eclogite garnets from Nordfjord, West Norway. *Contributions to Mineralogy and Petrology*, *32*(2), 112-125. https://doi.org/10.1007/BF00383054

Campomenosi, N., Mazzucchelli, M. L., Mihailova, B., Scambelluri, M., Angel, R. J., Nestola, F., Reali, A., & Alvaro, M. (2018). How geometry and anisotropy affect residual strain in host-inclusion systems : Coupling experimental and numerical approaches. *American Mineralogist*, *103*(12), 2032-2035. https://doi.org/10.2138/am-2018-6700CCBY

Carignan, J., Hild, P., Mevelle, G., Morel, J., & Yeghicheyan, D. (2001). Routine Analyses of Trace Elements in Geological Samples using Flow Injection and Low Pressure On-Line Liquid Chromatography Coupled to ICP-MS : A Study of Geochemical Reference Materials BR, DR-N, UB-N, AN-G and GH. *Geostandards Newsletter*, *25*(2-3), 187-198. https://doi.org/10.1111/j.1751-908X.2001.tb00595.x

Carswell, D. A., Brueckner, H. K., Cuthbert, S. J., Mehta, K., & O'Brien, P. J. (2003). The timing of stabilisation and the exhumation rate for ultra-high pressure rocks in the Western Gneiss Region of Norway. *Journal of Metamorphic Geology*, *21*(6), 601-612. https://doi.org/10.1046/j.1525-1314.2003.00467.x

Carswell, D. A., Cuthbert, S. J., & Krogh Ravna, E. J. (1999). Ultrahigh-Pressure Metamorphism in the Western Gneiss Region of the Norwegian Caledonides. *International Geology Review*, *41*(11), 955-966. https://doi.org/10.1080/00206819909465182

Carswell, D. A., Tucker, R. D., O'Brien, P. J., & Krogh, T. E. (2003). Coesite micro-inclusions and the U/Pb age of zircons from the Hareidland Eclogite in the Western Gneiss Region of Norway. *Lithos*, *67*(3-4), 181-190. https://doi.org/10.1016/S0024-4937(03)00014-8

Carswell, D. A., Wilson, R. N., & Zhai, M. (1996). Ultra-high pressure aluminous titanites in carbonate-bearing eclogites at Shuanghe in Dabieshan, central China. *Mineralogical Magazine*, *60*(400), 461-471. https://doi.org/10.1180/minmag.1996.060.400.07

Carter, I. S. M., Parsons, A., Waters, D. J., & Gopon, P. (2021). *Exhumation History of the Western Gneiss Region Revealed Through Symplectite Thermobarometry*. EGU General Assembly, Vienna. https://doi.org/10.5194/egusphere-egu21-1364

Chauvet, A., Kienast, J. R., Pinardon, J. L., & Brunel, M. (1992). Petrological constraints and PT path of Devonian collapse tectonics within the Scandian mountain belt (Western Gneiss Region, Norway). *Journal of the Geological Society*, *149*, 383-400.

Clarke, G. L., Powell, R., & Fitzherbert, J. A. (2006). The lawsonite paradox : A comparison of field evidence and mineral equilibria modelling. *Journal of Metamorphic Geology*, *24*(8), 715-725. https://doi.org/10.1111/j.1525-1314.2006.00664.x

Corfu, F., & Andersen, T. B. (2002). U–Pb ages of the Dalsfjord Complex, SW Norway, and their bearing on the correlation of allochthonous crystalline segments of the Scandinavian Caledonides. *International Journal of Earth Sciences*, *91*(6), 955-963. https://doi.org/10.1007/s00531-002-0298-3

Corfu, F., Austrheim, H., & Ganzhorn, A.-C. (2014). Localized granulite and eclogite facies metamorphism at Flatraket and Kråkeneset, Western Gneiss Region : U–Pb data and tectonic implications. *Geological Society, London, Special Publications*, *390*(1), 425-442. https://doi.org/10.1144/SP390.22

Cuthbert, S. J., Carswell, D. A., Krogh-Ravna, E. J., & Wain, A. (2000). Eclogites and eclogites in the Western Gneiss Region, Norwegian Caledonides. *Lithos*, *52*(1-4), 165-195. https://doi.org/10.1016/S0024-4937(99)00090-0

Cutts, J. A., & Smit, M. A. (2018). Rates of Deep Continental Burial From Lu-Hf Garnet Chronology and Zr-in-Rutile Thermometry on (Ultra)high-Pressure Rocks. *Tectonics*, *37*(1), 71-88. https://doi.org/10.1002/2017TC004723

Cutts, J. A., Smit, M. A., & Vrijmoed, J. C. (2020). Evidence for non-lithostatic pressure in subducted continental crust. *Contributions to Mineralogy and Petrology*, *175*(3). https://doi.org/10.1007/s00410-019-1633-z

de Capitani, C., & Petrakakis, K. (2010). The computation of equilibrium assemblage diagrams with Theriak/Domino software. *American Mineralogist*, *95*(7), 1006-1016. https://doi.org/10.2138/am.2010.3354

Dewey, J. F., Ryan, P. D., & Andersen, T. B. (1993). Orogenic uplift and collapse, crustal thickness, fabrics and metamorphic phase changes : The role of eclogites. *Geological Society, London, Special Publications*, *76*(1), 325-343. https://doi.org/10.1144/GSL.SP.1993.076.01.16

Dobrzhinetskaya, L. F., Eide, E. A., Larsen, R. B., Sturt, B. A., Trønnes, R. G., Smith, D. C., Taylor, W. R., & Posukhova, T. V. (1995). Microdiamond in high-grade metamorphic rocks of the Western Gneiss region, Norway. *Geology*, *23*(7), 597-600.

Duretz, T., Gerya, T. V., Kaus, B. J. P., & Andersen, T. B. (2012). Thermomechanical modeling of slab eduction. *Journal of Geophysical Research: Solid Earth*, *117*(B08411). https://doi.org/10.1029/2012JB009137

Enami, M., Zang, Q., & Yin, Y. (1993). High-pressure eclogites in northern Jiangsu – southern Shandong province, eastern China. *Journal of Metamorphic Geology*, *11*(4), 589-603. https://doi.org/10.1111/j.1525-1314.1993.tb00174.x

Engvik, A. K., & Andersen, T. B. (2000). Evolution of Caledonian deformation fabrics under eclogite and amphibolite facies at Vårdalsneset, Western Gneiss Region, Norway. *Journal of Metamorphic Geology*, *18*(3), 241-257. https://doi.org/10.1046/j.1525-1314.2000.00252.x

Ernst, W. G. (2001). Subduction, ultrahigh-pressure metamorphism, and regurgitation of buoyant crustal slices—Implications for arcs and continental growth. *Physics of the Earth and Planetary Interiors*, *127*(1), 253-275. https://doi.org/10.1016/S0031-9201(01)00231-X

Evans, B. W. (1990). Phase relations of epidote-blueschists. *Lithos*, *25*(1-3), 3-23. https://doi.org/10.1016/0024-4937(90)90003-J

Faccenda, M., Minelli, G., & Gerya, T. V. (2009). Coupled and decoupled regimes of continental collision : Numerical modeling. *Earth and Planetary Science Letters*, *278*(3), 337-349. https://doi.org/10.1016/j.epsl.2008.12.021

Faryad, S. W., Ježek, J., & Kulhánek, J. (2022). Constraining the P–T path of (U)HP rocks with reaction overstepping during subduction; example from the Western Gneiss Region (Norway). *Journal of Metamorphic Geology*, *n/a*(n/a). https://doi.org/10.1111/jmg.12680

Fauconnier, J., Labrousse, L., Andersen, T. B., Beyssac, O., Duprat-Oualid, S., & Yamato, P. (2014). Thermal structure of a major crustal shear zone, the basal thrust in the Scandinavian Caledonides. *Earth and Planetary Science Letters*, *385*, 162-171. https://doi.org/10.1016/j.epsl.2013.10.038

Feenstra, A., Petrakakis, K., & Rhede, D. (2007). Variscan relicts in Alpine high-P pelitic rocks from Samos (Greece) : Evidence from multi-stage garnet and its included minerals. *Journal of Metamorphic Geology*, *25*(9), 1011-1033. https://doi.org/10.1111/j.1525-1314.2007.00741.x

Ferry, J. M., & Watson, E. B. (2007). New thermodynamic models and revised calibrations for the Ti-in-zircon and Zr-in-rutile thermometers. *Contributions to Mineralogy and Petrology*, *154*(4), 429-437. https://doi.org/10.1007/s00410-007-0201-0

Fossen, H. (1992). The role of extensional tectonics in the Caledonides of south Norway. *Journal of Structural Geology*, *14*(8-9), 1033-1046. https://doi.org/10.1016/0191-8141(92)90034-T

Fossen, H., & Dallmeyer, R. D. (1998). 40Ar/39Ar muscovite dates from the nappe region of southwestern Norway : Dating extensional deformation in the Scandinavian Caledonides. *Tectonophysics*, *285*(1-2), 119-133. https://doi.org/10.1016/S0040-1951(97)00187-X

Ganzhorn, A. C., Labrousse, L., Prouteau, G., Leroy, C., Vrijmoed, J. C., Andersen, T. B., & Arbaret, L. (2014). Structural, petrological and chemical analysis of syn-kinematic migmatites : Insights from the Western Gneiss Region, Norway. *Journal of Metamorphic Geology*, *32*(6), 647-673. https://doi.org/10.1111/jmg.12084

Gee, D. G. (1975). A tectonic model for the central part of the Scandinavian Caledonides. *American Journal of Science*, *275*(A), 468-515.

Gee, D. G., Janák, M., Majka, J., Robinson, P., & van Roermund, H. (2013). Subduction along and within the Baltoscandian margin during closing of the Iapetus Ocean and Baltica-Laurentia collision. *Lithosphere*, *5*(2), 169-178. https://doi.org/10.1130/L220.1

Gerya, T. (2015). Tectonic overpressure and underpressure in lithospheric tectonics and metamorphism. *Journal of Metamorphic Geology*, *33*(8), 785-800. https://doi.org/10.1111/jmg.12144

Gjelsvik, T. (1951). Oversikt over bergartene på Sunnmøre og tilgrensende deler av Nordfjord. Med geologisk oversiktskart av T. Gjelsvik & Chr. C. Gleditsch. *Norges Geologiske Undersøkelse*, *179*, 46.

Green, E. C. R., White, R. W., Diener, J. F. A., Powell, R., Holland, T. J. B., & Palin, R. M. (2016). Activity–composition relations for the calculation of partial melting equilibria in metabasic rocks. *Journal of Metamorphic Geology*, *34*(9), 845-869. https://doi.org/10.1111/jmg.12211

Griffin, W. L., Austrheim, H., Brastad, K., Bryhni, I., Krill, A. G., Krogh, E. J., Mørk, M. B. E., Qvale, H., & Tørudbakken, B. (1985). High-pressure metamorphism in the Scandinavian Caledonides. In *Gee, D.G., Sturt, B.A. (Eds.), The Caledonide Orogen—Scandinavia and Related Areas* (p. 783-801). Wiley.

Griffin, W. L., & Brueckner, H. K. (1985). REE, Rb–Sr and Sm–Nd studies of Norwegian eclogites. *Chemical Geology (Isotope Geoscience Section)*, *52*, 249-271. https://doi.org/10.1016/0168-9622(85)90021-1

Hacker, B. R. (2006). Pressures and Temperatures of Ultrahigh-Pressure Metamorphism : Implications for UHP Tectonics and H2O in Subducting Slabs. *International Geology Review*, *48*(12), 1053-1066. https://doi.org/10.2747/0020-6814.48.12.1053

Hacker, B. R., Andersen, T. B., Johnston, S., Kylander-Clark, A. R. C., Peterman, E. M., Walsh, E. O., & Young, D. (2010). High-temperature deformation during continental-margin subduction & exhumation : The ultrahigh-pressure Western Gneiss Region of Norway. *Tectonophysics*, *480*(1-4), 149-171. https://doi.org/10.1016/j.tecto.2009.08.012

Hacker, B. R., Andersen, T. B., Root, D. B., Mehl, L., Mattinson, J. M., & Wooden, J. L. (2003). Exhumation of high-pressure rocks beneath the Solund Basin, Western Gneiss Region of Norway. *Journal of Metamorphic Geology*, *21*(6), 613-629. https://doi.org/10.1046/j.1525-1314.2003.00468.x

Hacker, B. R., & Gans, P. B. (2005). Continental collisions and the creation of ultrahigh-pressure terranes : Petrology and thermochronology of nappes in the central Scandinavian Caledonides. *Geological Society of America Bulletin*, *117*(1), 117. https://doi.org/10.1130/B25549.1

Holland, T., & Blundy, J. (1994). Non-ideal interactions in calcic amphiboles and their bearing on amphibole-plagioclase thermometry. *Contributions to Mineralogy and Petrology*, *116*(4), 433-447. https://doi.org/10.1007/BF00310910

Holland, T. J. B., & Powell, R. (2011). An improved and extended internally consistent thermodynamic dataset for phases of petrological interest, involving a new equation of state for solids. *Journal of Metamorphic Geology*, *29*(3), 333-383. https://doi.org/10.1111/j.1525-1314.2010.00923.x

Holland, T., & Powell, R. (2003). Activity–composition relations for phases in petrological calculations : An asymmetric multicomponent formulation. *Contributions to Mineralogy and Petrology*, *145*(4), 492-501. https://doi.org/10.1007/s00410-003-0464-z

Hollocher, K., Robinson, P., Terry, M. P., & Walsh, E. (2007). Application of major- and trace-element geochemistry to refine U-Pb zircon, and Sm/Nd or Lu/Hf sampling targets for geochronology of HP and UHP eclogites, Western Gneiss Region, Norway. *American Mineralogist*, *92*(11-12), 1919-1924. https://doi.org/10.2138/am.2007.2405

Jakob, J., Alsaif, M., Corfu, F., & Andersen, T. B. (2017). Age and origin of thin discontinuous gneiss sheets in the distal domain of the magma-poor hyperextended pre-Caledonian margin of Baltica, southern Norway. *Journal of the Geological Society*, *174*, 557-571.

Jamtveit, B. (1987). Metamorphic evolution of the Eiksunddal eclogite complex. Western Norway, and some tectonic implications. *Contributions to Mineralogy and Petrology*, *95*(1), 82-99. https://doi.org/10.1007/BF00518032

Jamtveit, B., Moulas, E., Andersen, T. B., Austrheim, H., Corfu, F., Petley-Ragan, A., & Schmalholz, S. M. (2018). High Pressure Metamorphism Caused by Fluid Induced Weakening of Deep Continental Crust. *Scientific Reports*, *8*(1), 17011. https://doi.org/10.1038/s41598-018-35200-1

Janák, M., Ravna, E. J. K., & Kullerud, K. (2012). Constraining peak P–T conditions in UHP eclogites : Calculated phase equilibria in kyanite- and phengite-bearing eclogite of the Tromsø Nappe, Norway. *Journal of Metamorphic Geology*, *30*(4), 377-396. https://doi.org/10.1111/j.1525-1314.2011.00971.x

Johnston, S. M., Hacker, B. R., & Andersen, T. B. (2007). Exhuming Norwegian ultrahigh-pressure rocks : Overprinting extensional structures and the role of the Nordfjord-Sogn Detachment Zone. *Tectonics*, *26*(TC5001), 12. https://doi.org/10.1029/2005TC001933

Johnston, S. M., Hacker, B. R., & Ducea, M. N. (2007). Exhumation of ultrahigh-pressure rocks beneath the Hornelen segment of the Nordfjord-Sogn Detachment Zone, western Norway. *Geological Society of America Bulletin*, *119*(9-10), 1232-1248. https://doi.org/10.1130/B26172.1

Klonowska, I., Janák, M., Majka, J., Froitzheim, N., & Kośmińska, K. (2016). Eclogite and garnet pyroxenite from Stor Jougdan, Seve Nappe Complex, Sweden : Implications for UHP metamorphism of allochthons in the Scandinavian Caledonides. *Journal of Metamorphic Geology*, *34*(2), 103-119. https://doi.org/10.1111/jmg.12173

Konrad-Schmolke, M., Zack, T., O'Brien, P. J., & Jacob, D. E. (2008). Combined thermodynamic and rare earth element modelling of garnet growth during subduction : Examples from ultrahigh-pressure eclogite of the Western Gneiss Region, Norway. *Earth and Planetary Science Letters*, *272*(1), 488-498. https://doi.org/10.1016/j.epsl.2008.05.018

Krabbendam, M., & Dewey, J. F. (1998). Exhumation of UHP rocks by transtension in the Western Gneiss Region, Scandinavian Caledonides. *Geological Society, London, Special Publications*, *135*(1), 159-181. https://doi.org/10.1144/GSL.SP.1998.135.01.11

Krabbendam, M., & Wain, A. (1997). Late-Caledonian structures, differential retrogression and structural position of (ultra)high-pressure rocks in the Nordfjord—Stadlandet area, Western Gneiss Region. *Norges Geologiske Undersøkelse Bulletin*, *432*, 127-139.

Krabbendam, M., Wain, A., & Andersen, T. B. (2000). Pre-Caledonian granulite and gabbro enclaves in the Western Gneiss Region, Norway : Indications of incomplete transition at high pressure. *Geological Magazine*, *137*(3), 235-255. https://doi.org/10.1017/S0016756800004015

Krogh, E. J. (1977). Evidence of Precambrian continent–continent collision in Western Norway. *Nature*, *267*(5606), 17-19. https://doi.org/10.1038/267017a0

Krogh, E. J. (1982). Metamorphic evolution of Norwegian country-rock eclogites, as deduced from mineral inclusions and compositional zoning in garnets. *Lithos*, *15*(4), 305-321. https://doi.org/10.1016/0024-4937(82)90021-4

Krogh Ravna, E. J., & Terry, M. P. (2004). Geothermobarometry of UHP and HP eclogites and schists—An evaluation of equilibria among garnet-clinopyroxene-kyanite-phengite-coesite/quartz. *Journal of Metamorphic Geology*, *22*(6), 579-592. https://doi.org/10.1111/j.1525-1314.2004.00534.x

Kylander-Clark, A. R. C., & Hacker, B. R. (2014). Age and significance of felsic dikes from the UHP western gneiss region. *Tectonics*, *33*(12), 2342-2360. https://doi.org/10.1002/2014TC003582

Kylander-Clark, A. R. C., Hacker, B. R., Johnson, C. M., Beard, B. L., & Mahlen, N. J. (2009). Slow subduction of a thick ultrahigh-pressure terrane. *Tectonics*, *28*(TC2003). https://doi.org/10.1029/2007TC002251

Kylander-Clark, A. R. C., Hacker, B. R., & Mattinson, J. M. (2008). Slow exhumation of UHP terranes : Titanite and rutile ages of the Western Gneiss Region, Norway. *Earth and Planetary Science Letters*, *272*(3-4), 531-540. https://doi.org/10.1016/j.epsl.2008.05.019

Labrousse, L. (2001). *L'exhumation des roches métamorphiques de très haute pression : Le cas des Calédonides de Norvège* [Thèse de doctorat]. Université de Paris 6.

Labrousse, L., Jolivet, L., Andersen, T. B., Agard, P., Hébert, R., Maluski, H., & Schärer, U. (2004). Pressure-temperature-time deformation history of the exhumation of ultra-high pressure rocks in the Western Gneiss Region, Norway. *Geological Society of America Special Paper*, *380*, 155-183.

Labrousse, L., Prouteau, G., & Ganzhorn, A.-C. (2011). Continental exhumation triggered by partial melting at ultrahigh pressure. *Geology*, *39*(12), 1171-1174. https://doi.org/10.1130/G32316.1

Le Bayon, B., Pitra, P., Ballevre, M., & Bohn, M. (2006). Reconstructing P–T paths during continental collision using multi-stage garnet (Gran Paradiso nappe, Western Alps). *Journal of Metamorphic Geology*, *24*(6), 477-496. https://doi.org/10.1111/j.1525-1314.2006.00649.x

Leake, B. E., Woolley, A. R., Arps, C. E. S., Birch, W. D., Gilbert, M. C., Grice, J. D., Hawthorne, F. C., Kato, A., Kisch, H. J., Krivovichev, V. G., Linthout, K., Laird, J., Mandarino, J. A., Maresch, W. V., Nickel, E. H., Rock, N. M. S., Schumacher, J. C., Smith, D. C., Stephenson, N. C. N., … Guo Youzhi. (1997). Nomenclature of amphiboles; report of the subcommittee on amphiboles of the International Mineralogical Association, Commission on New Minerals and Mineral Names. *The Canadian Mineralogist*, *35*(1), 219-246.

Li, Z. H., Gerya, T. V., & Burg, J.-P. (2010). Influence of tectonic overpressure on *P-T* paths of HP-UHP rocks in continental collision zones : Thermomechanical modelling. *Journal of Metamorphic Geology*, *28*(3), 227-247. https://doi.org/10.1111/j.1525-1314.2009.00864.x

López-Carmona, A., Pitra, P., & Abati, J. (2013). Blueschist-facies metapelites from the Malpica–Tui Unit (NW Iberian Massif) : Phase equilibria modelling and H2O and Fe2O3 influence in high-pressure assemblages. *Journal of Metamorphic Geology*, *31*(3), 263-280. https://doi.org/10.1111/jmg.12018

Luisier, C., Baumgartner, L., Schmalholz, S. M., Siron, G., & Vennemann, T. (2019). Metamorphic pressure variation in a coherent Alpine nappe challenges lithostatic pressure paradigm. *Nature Communications*, *10*(1), 4734. https://doi.org/10.1038/s41467-019-12727-z

Luvizotto, G. L., Zack, T., Meyer, H. P., Ludwig, T., Triebold, S., Kronz, A., Münker, C., Stockli, D. F., Prowatke, S., Klemme, S., Jacob, D. E., & von Eynatten, H. (2009). Rutile crystals as potential trace

element and isotope mineral standards for microanalysis. *Chemical Geology*, *261*(3), 346-369. https://doi.org/10.1016/j.chemgeo.2008.04.012

Majka, J., Rosén, Å., Janák, M., Froitzheim, N., Klonowska, I., Manecki, M., Sasinková, V., & Yoshida, K. (2014). Microdiamond discovered in the Seve Nappe (Scandinavian Caledonides) and its exhumation by the "vacuum-cleaner" mechanism. *Geology*, *42*(12), 1107-1110. https://doi.org/10.1130/G36108.1

Mancktelow, N. S. (2008). Tectonic pressure : Theoretical concepts and modelled examples. *Lithos*, *103*(1-2), 149-177. https://doi.org/10.1016/j.lithos.2007.09.013

Manzotti, P., & Ballèvre, M. (2013). Multistage garnet in high-pressure metasediments : Alpine overgrowths on Variscan detrital grains. *Geology*, *41*(11), 1151-1154. https://doi.org/10.1130/G34741.1

Manzotti, P., Ballèvre, M., Pitra, P., & Schiavi, F. (2021). Missing lawsonite and aragonite found : P–T and fluid composition in meta-marls from the Combin Zone (Western Alps). *Contributions to Mineralogy and Petrology*, *176*(8), 60. https://doi.org/10.1007/s00410-021-01818-0

March, S., Hand, M., Tamblyn, R., Carvalho, B. B., & Clark, C. (2022). A diachronous record of metamorphism in metapelites of the Western Gneiss Region, Norway. *Journal of Metamorphic Geology*, *n/a*(n/a). https://doi.org/10.1111/jmg.12660

Masago, H. (2000). Metamorphic petrology of the Barchi-Kol metabasites, western Kokchetav ultrahigh-pressure-high-pressure massif, northern Kazakhstan. *The Island Arc*, *9*(3), 358-378. https://doi.org/10.1046/j.1440-1738.2000.00283.x

Mazzucchelli, M. L., Angel, R. J., & Alvaro, M. (2021). EntraPT : An online platform for elastic geothermobarometry. *American Mineralogist*, *106*(5), 830-837. https://doi.org/10.2138/am-2021-7693CCBYNCND

Medaris, L. G., Brueckner, H. K., Cai, Y., Griffin, W. L., & Janák, M. (2018). Eclogites in peridotite massifs in the Western Gneiss Region, Scandinavian Caledonides : Petrogenesis and comparison with those in the Variscan Moldanubian Zone. *Lithos*, *322*, 325-346. https://doi.org/10.1016/j.lithos.2018.10.013

Milani, S., Angel, R. J., Scandolo, L., Mazzucchelli, M. L., Ballaran, T. B., Klemme, S., Domeneghetti, M. C., Miletich, R., Scheidl, K. S., Derzsi, M., Tokár, K., Prencipe, M., Alvaro, M., & Nestola, F. (2017). Thermo-elastic behavior of grossular garnet at high pressures and temperatures. *American Mineralogist*, *102*(4), 851-859. https://doi.org/10.2138/am-2017-5855

Milani, S., Nestola, F., Alvaro, M., Pasqual, D., Mazzucchelli, M. L., Domeneghetti, M. C., & Geiger, C. A. (2015). Diamond–garnet geobarometry : The role of garnet compressibility and expansivity. *Lithos*, *227*, 140-147. https://doi.org/10.1016/j.lithos.2015.03.017

Miyashiro, A. (1972). Metamorphism and related magmatism in plate tectonics. *American Journal of Science*, *272*(7), 629-656. https://doi.org/10.2475/ajs.272.7.629

Moulas, E., Burg, J.-P., & Podladchikov, Y. (2014). Stress field associated with elliptical inclusions in a deforming matrix : Mathematical model and implications for tectonic overpressure in the lithosphere. *Tectonophysics*, *631*, 37-49. https://doi.org/10.1016/j.tecto.2014.05.004

Nosenzo, F., Manzotti, P., Poujol, M., Ballèvre, M., & Langlade, J. (2022). A window into an older orogenic cycle : P–T conditions and timing of the pre-Alpine history of the Dora-Maira Massif

(Western Alps). *Journal of Metamorphic Geology*, *40*(4), 789-821. https://doi.org/10.1111/jmg.12646

Pan, R., Macris, C. A., & Menold, C. A. (2020). Thermodynamic modeling of high-grade metabasites : A case study using the Tso Morari UHP eclogite. *Contributions to Mineralogy and Petrology*, *175*(78), 28. https://doi.org/10.1007/s00410-020-01717-w

Paquette, J.-L., Piro, J.-L., Devidal, J.-L., Bosse, V., Didier, A., Sannac, S., & Abdelnour, Y. (2014). Sensitivity Enhancement in LA-ICP-MS by N2 Addition to Carrier Gas : Application to Radiometric Dating of U-Th-Bearing Minerals. *Agilent ICP-MS Journal*, *58*, 4-5.

Paton, C., Hellstrom, J., Paul, B., Woodhead, J., & Hergt, J. (2011). Iolite : Freeware for the visualisation and processing of mass spectrometric data. *Journal of Analytical Atomic Spectrometry*, *26*(12), 2508. https://doi.org/10.1039/c1ja10172b

Penniston-Dorland, S. C., Kohn, M. J., & Manning, C. E. (2015). The global range of subduction zone thermal structures from exhumed blueschists and eclogites : Rocks are hotter than models. *Earth and Planetary Science Letters*, *428*, 243-254. https://doi.org/10.1016/j.epsl.2015.07.031

Peterman, E. M., Hacker, B. R., & Baxter, E. F. (2009). Phase transformations of continental crust during subduction and exhumation : Western Gneiss Region, Norway. *European Journal of Mineralogy*, *21*(6), 1097-1118. https://doi.org/10.1127/0935-1221/2009/0021-1988

Petrini & Podladchikov. (2000). Lithospheric pressure–depth relationship in compressive regions of thickened crust. *Journal of Metamorphic Geology*, *18*(1), 67-77. https://doi.org/10.1046/j.1525-1314.2000.00240.x

Pitra, P., Boulvais, P., Antonoff, V., & Diot, H. (2008). Wagnerite in a cordierite-gedrite gneiss : Witness of long-term fluid-rock interaction in the continental crust (Ile d'Yeu, Armorican Massif, France). *American Mineralogist*, *93*(2-3), 315-326. https://doi.org/10.2138/am.2008.2597

Powell, R., & Holland, T. J. B. (1988). An internally consistent dataset with uncertainties and correlations : 3. Applications to geobarometry, worked examples and a computer program. *Journal of Metamorphic Geology*, *6*(2), 173-204. https://doi.org/10.1111/j.1525-1314.1988.tb00415.x

Renedo, R. N., Nachlas, W. O., Whitney, D. L., Teyssier, C., Piazolo, S., Gordon, S. M., & Fossen, H. (2015). Fabric development during exhumation from ultrahigh-pressure in an eclogite-bearing shear zone, Western Gneiss Region, Norway. *Journal of Structural Geology*, *71*, 58-70. https://doi.org/10.1016/j.jsg.2014.09.012

Reuber, G., Kaus, B. J. P., Schmalholz, S. M., & White, R. W. (2016). Nonlithostatic pressure during subduction and collision and the formation of (ultra)high-pressure rocks. *Geology*, *44*(5), 343-346. https://doi.org/10.1130/G37595.1

Roberts, D. (2003). The Scandinavian Caledonides : Event chronology, palaeogeographic settings and likely modern analogues. *Tectonophysics*, *365*(1), 283-299. https://doi.org/10.1016/S0040-1951(03)00026-X

Roberts, D., & Gee, D. G. (1985). An introduction to the structure of the Scandinavian Caledonides. In *Gee, D.G., Sturt, B.A. (Eds.), The Caledonide Orogen—Scandinavia and Related Areas* (p. 55-68). Wiley.

Roberts, D., Melezhik, V. M., & Heldal, T. (2002). Carbonate formations and early NW-directed thrusting in the highest allochthons of the Norwegian Caledonides : Evidence of a Laurentian

ancestry. *Journal of the Geological Society*, *159*(2), 117-120. https://doi.org/10.1144/0016-764901-128

Root, D. B., Hacker, B. R., Gans, P. B., Ducea, M. N., Eide, E. A., & Mosenfelder, J. L. (2005). Discrete ultrahigh-pressure domains in the Western Gneiss Region, Norway : Implications for formation and exhumation. *Journal of Metamorphic Geology*, *23*(1), 45-61. https://doi.org/10.1111/j.1525-1314.2005.00561.x

Root, D. B., Hacker, B. R., Mattinson, J. M., & Wooden, J. L. (2004). Zircon geochronology and ca. 400 Ma exhumation of Norwegian ultrahigh-pressure rocks : An ion microprobe and chemical abrasion study. *Earth and Planetary Science Letters*, *228*(3-4), 325-341. https://doi.org/10.1016/j.epsl.2004.10.019

Schärer, U., & Labrousse, L. (2003). Dating the exhumation of UHP rocks and associated crustal melting in the Norwegian Caledonides. *Contributions to Mineralogy and Petrology*, *144*(6), 758-770. https://doi.org/10.1007/s00410-002-0428-8

Schmalholz, S. M., & Podladchikov, Y. Y. (2013). Tectonic overpressure in weak crustal-scale shear zones and implications for the exhumation of high-pressure rocks. *Geophysical Research Letters*, *40*(10), 1984-1988. https://doi.org/10.1002/grl.50417

Schumacher, J. C., Brady, J. B., Cheney, J. T., & Tonnsen, R. R. (2008). Glaucophane-bearing Marbles on Syros, Greece. *Journal of Petrology*, *49*(9), 1667-1686. https://doi.org/10.1093/petrology/egn042

Skelton, A., Peillod, A., Glodny, J., Klonowska, I., Månbro, C., Lodin, K., & Ring, U. (2019). Preservation of high-*P* rocks coupled to rock composition and the absence of metamorphic fluids. *Journal of Metamorphic Geology*, *37*(3), 359-381. https://doi.org/10.1111/jmg.12466

Smith, D. C. (1984). Coesite in clinopyroxene in the Caledonides and its implications for geodynamics. *Nature*, *310*(5979), 641-644. https://doi.org/10.1038/310641a0

Smith, D. C., & Lappin, M. A. (1989). Coesite in the Straumen kyanite-eclogite pod, Norway. *Terra Nova*, *1*(1), 47-56. https://doi.org/10.1111/j.1365-3121.1989.tb00325.x

Spandler, C., Hermann, J., Arculus, R., & Mavrogenes, J. (2003). Redistribution of trace elements during prograde metamorphism from lawsonite blueschist to eclogite facies; implications for deep subduction-zone processes. *Contributions to Mineralogy and Petrology*, *146*(2), 205-222. https://doi.org/10.1007/s00410-003-0495-5

Spencer, K. J., Hacker, B. R., Kylander-Clark, A. R. C., Andersen, T. B., Cottle, J. M., Stearns, M. A., Poletti, J. E., & Seward, G. G. E. (2013). Campaign-style titanite U–Pb dating by laser-ablation ICP : Implications for crustal flow, phase transformations and titanite closure. *Chemical Geology*, *341*, 84-101. https://doi.org/10.1016/j.chemgeo.2012.11.012

Stepanov, A. S., Rubatto, D., Hermann, J., & Korsakov, A. V. (2016). Contrasting *P-T* paths within the Barchi-Kol UHP terrain (Kokchetav Complex) : Implications for subduction and exhumation of continental crust. *American Mineralogist*, *101*(4), 788-807. https://doi.org/10.2138/am-2016-5454

Stephens, M. B., & Gee, D. G. (1989). Terranes and polyphase accretionary history in the Scandinavian Caledonides. *Geological Society of America Special Paper*, *230*, 17-30.

Straume & Austrheim. (1999). Importance of fracturing during retro-metamorphism of eclogites. *Journal of Metamorphic Geology*, *17*(6), 637-652. https://doi.org/10.1046/j.1525-1314.1999.00218.x

Sun, S. S., & McDonough, W. F. (1989). Chemical and isotopic systematics of oceanic basalts : Implications for mantle composition and processes. *Geological Society, London, Special Publications*, *42*(1), 313-345.

Syracuse, E. M., van Keken, P. E., & Abers, G. A. (2010). The global range of subduction zone thermal models. *Physics of the Earth and Planetary Interiors*, *183*(1-2), 73-90. https://doi.org/10.1016/j.pepi.2010.02.004

Tajčmanová, L., Manzotti, P., & Alvaro, M. (2021). Under Pressure : High-Pressure Metamorphism in the Alps. *Elements*, *17*(1), 17-22. https://doi.org/10.2138/gselements.17.1.17

Tajčmanová, L., Vrijmoed, J. C., & Moulas, E. (2015). Grain-scale pressure variations in metamorphic rocks : Implications for the interpretation of petrographic observations. *Lithos*, *216-217*, 338-351. https://doi.org/DOI: 10.1016/j.lithos.2015.01.006

Tamblyn, R., Hand, M., Simpson, A., Gilbert, S., Wade, B., & Glorie, S. (2021). In situ laser ablation Lu–Hf geochronology of garnet across the Western Gneiss Region : Campaign-style dating of metamorphism. *Journal of the Geological Society*, jgs2021-094. https://doi.org/10.1144/jgs2021-094

Terry, M. P., Robinson, P., & Ravna, E. J. K. (2000). Kyanite eclogite thermobarometry and evidence for thrusting of UHP over HP metamorphic rocks, Nordøyane, Western Gneiss Region, Norway. *American Mineralogist*, *85*(11-12), 1637-1650. https://doi.org/10.2138/am-2000-11-1207

Thomas, J. B., & Spear, F. S. (2018). Experimental study of quartz inclusions in garnet at pressures up to 3.0 GPa : Evaluating validity of the quartz-in-garnet inclusion elastic thermobarometer. *Contributions to Mineralogy and Petrology*, *173*(42). https://doi.org/10.1007/s00410-018-1469-y

Thompson, A. B., & Connolly, J. A. D. (1990). Metamorphic fluids and anomalous porosities in the lower crust. *Tectonophysics*, *182*(1), 47-55. https://doi.org/10.1016/0040-1951(90)90341-5

Tomkins, H. S., Powell, R., & Ellis, D. J. (2007). The pressure dependence of the zirconium-in-rutile thermometer. *Journal of Metamorphic Geology*, *25*(6), 703-713. https://doi.org/10.1111/j.1525-1314.2007.00724.x

Troitzsch, U., & Ellis, D. J. (2002). Thermodynamic properties and stability of AlF-bearing titanite CaTiOSiO4–CaAlFSiO4. *Contributions to Mineralogy and Petrology*, *142*(5), 543-563. https://doi.org/10.1007/s004100100309

van Roermund, H. L. M., Carswell, D. A., Drury, M. R., & Heijboer, T. C. (2002). Microdiamonds in a megacrystic garnet websterite pod from Bardane on the island of Fjørtoft, western Norway : Evidence for diamond formation in mantle rocks during deep continental subduction. *Geology*, *30*(11), 959-962. https://doi.org/10.1130/0091-7613(2002)030<0959:MIAMGW>2.0.CO;2

Vrijmoed, J. C., Podladchikov, Y. Y., Andersen, T. B., & Hartz, E. H. (2009). An alternative model for ultra-high pressure in the Svartberget Fe-Ti garnet-peridotite, Western Gneiss Region, Norway. *European Journal of Mineralogy*, *21*(6), 1119-1133. https://doi.org/10.1127/0935-1221/2009/0021-1985

Vrijmoed, J. C., Smith, D. C., & Van Roermund, H. L. M. (2008). Raman confirmation of microdiamond in the Svartberget Fe-Ti type garnet peridotite, Western Gneiss Region, Western Norway. *Terra Nova*, *20*(4), 295-301. https://doi.org/10.1111/j.1365-3121.2008.00820.x

Vrijmoed, J. C., Van Roermund, H. L. M., & Davies, G. R. (2006). Evidence for diamond-grade ultra-high pressure metamorphism and fluid interaction in the Svartberget Fe–Ti garnet peridotite–

websterite body, Western Gneiss Region, Norway. *Mineralogy and Petrology*, *88*(1-2), 381-405. https://doi.org/10.1007/s00710-006-0160-6

Wain, A. (1997). New evidence for coesite in eclogite and gneisses : Defining an ultrahigh-pressure province in the Western Gneiss region of Norway. *Geology*, *25*(10), 927-930.

Wain, A. L., Waters, D. J., & Austrheim, H. (2001). Metastability of granulites and processes of eclogitisation in the UHP region of western Norway. *Journal of Metamorphic Geology*, *19*(5), 609-625. https://doi.org/10.1046/j.0263-4929.2001.00333.x

Wain, A., Waters, D., Jephcoat, A., & Olijynk, H. (2000). The high-pressure to ultrahigh-pressure eclogite transition in the Western Gneiss Region, Norway. *European Journal of Mineralogy*, *12*(3), 667-687. https://doi.org/10.1127/0935-1221/2000/0012-0667

Walczak, K., Cuthbert, S., Kooijman, E., Majka, J., & Smit, M. A. (2019). U–Pb zircon age dating of diamond-bearing gneiss from Fjørtoft reveals repeated burial of the Baltoscandian margin during the Caledonian Orogeny. *Geological Magazine*, *156*(11), 1949-1964. https://doi.org/10.1017/S0016756819000268

Walsh, E. O., & Hacker, B. R. (2004). The fate of subducted continental margins : Two-stage exhumation of the high-pressure to ultrahigh-pressure Western Gneiss Region, Norway. *Journal of Metamorphic Geology*, *22*(7), 671-687. https://doi.org/10.1111/j.1525-1314.2004.00541.x

Warren, C. J. (2013). Exhumation of (ultra-)high-pressure terranes : Concepts and mechanisms. *Solid Earth*, *4*(1), 75-92. https://doi.org/10.5194/se-4-75-2013

White, R. W., Powell, R., & Holland, T. J. B. (2007). Progress relating to calculation of partial melting equilibria for metapelites. *Journal of Metamorphic Geology*, *25*(5), 511-527. https://doi.org/10.1111/j.1525-1314.2007.00711.x

White, R. W., Powell, R., Holland, T. J. B., Johnson, T. E., & Green, E. C. R. (2014). New mineral activity–composition relations for thermodynamic calculations in metapelitic systems. *Journal of Metamorphic Geology*, *32*(3), 261-286. https://doi.org/10.1111/jmg.12071

Wiest, J. D., Jacobs, J., Fossen, H., Ganerød, M., & Osmundsen, P. T. (2021). Segmentation of the Caledonian orogenic infrastructure and exhumation of the Western Gneiss Region during transtensional collapse. *Journal of the Geological Society*, *178*(3). https://doi.org/10.1144/jgs2020-199

Wilks, W. J., & Cuthbert, S. J. (1994). The evolution of the Hornelen Basin detachment system, western Norway : Implications for the style of late orogenic extension in the southern Scandinavian Caledonides. *Tectonophysics*, *238*(1), 1-30. https://doi.org/10.1016/0040-1951(94)90047-7

Yamato, P., & Brun, J. P. (2017). Metamorphic record of catastrophic pressure drops in subduction zones. *Nature Geoscience*, *10*(1), 46-50. https://doi.org/10.1038/ngeo2852

Young, D. J. (2018). Structure of the (ultra)high-pressure Western Gneiss Region, Norway : Imbrication during Caledonian continental margin subduction. *GSA Bulletin*, *130*(5-6), 926-940. https://doi.org/10.1130/B31764.1

Young, D. J., Hacker, B. R., Andersen, T. B., & Corfu, F. (2007). Prograde amphibolite facies to ultrahigh-pressure transition along Nordfjord, western Norway : Implications for exhumation tectonics. *Tectonics*, *26*, TC1007. https://doi.org/10.1029/2004TC001781

Zulbati, F. (2011). Multistage metamorphism and deformation in high-pressure metabasites of the northern Adula Nappe Complex (Central Alps, Switzerland). *Geological Journal*, *46*(1), 82-103. https://doi.org/10.1002/gj.1263

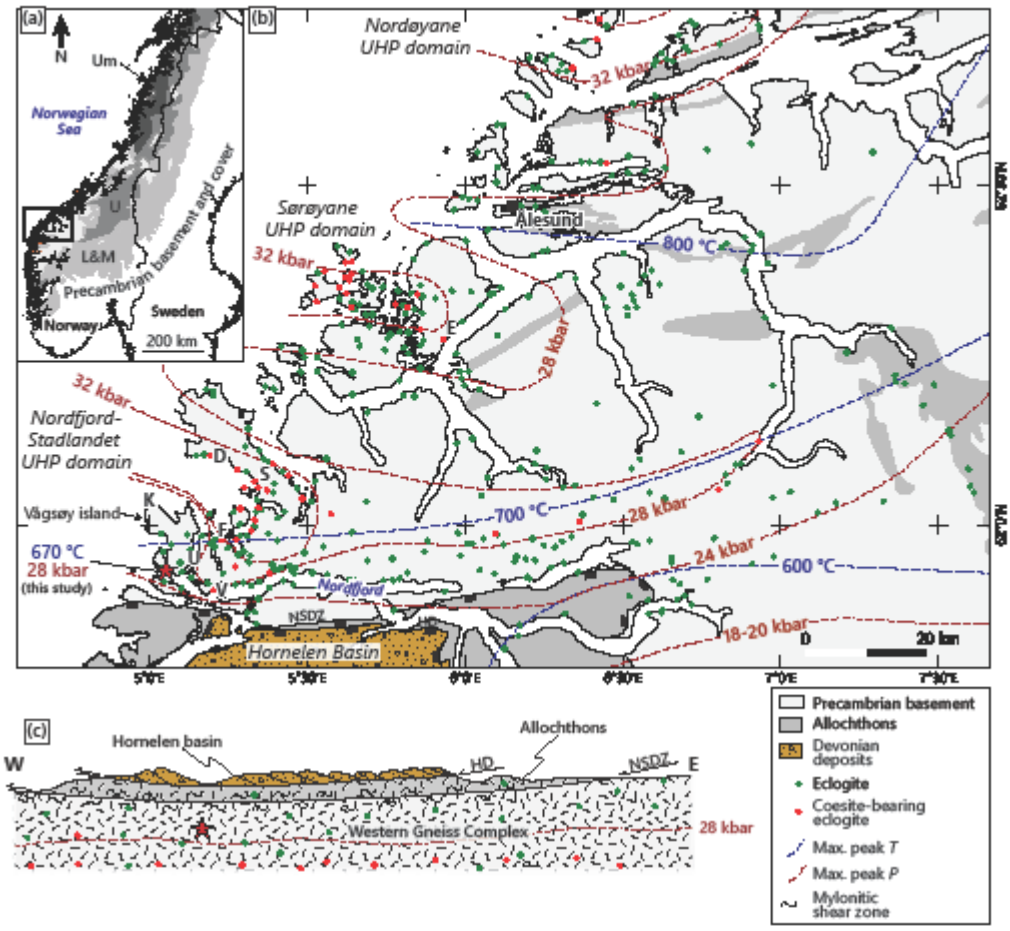

Figure 1. (a) Simplified map of Norway showing the location of the study area, modified after Gee et al. (2013). The lightest shade of grey corresponds to the allochthonous Precambrian basement. L&M: Lower & Middle Allochthons; U: Upper Allochthon; Um: Uppermost Allochthon. (b) Structural map of the study area. The red star shows the location of the studied sample from Vågsvåg on the Vågsøy island (WGS84: 61.93106N, 5.05121E) with the approximate peak P–T conditions inferred from our study. Approximate peak temperatures after Kylander-Clark et al. (2008), peak pressures after Hacker et al. (2010) and eclogite locations after Young (2018). (c) Schematic cross-section modified after Labrousse (2001) and Johnston, Hacker, & Andersen (2007). NSDZ: Nordfjord-Sogn Detachment Zone; HD: Hornelen Detachment. Locations referred to in the text are Flatraket (F), Kråkeneset (K), the Stadlandet peninsula (S), Drage (D), Verpeneset (V), Ulvesund (U) and Eiksund-dal (E).

Figure 1. (a) Simplified map of Norway showing the location of the study area, modified after Gee et al. (2013). The lightest shade of grey corresponds to the allochthonous Precambrian basement. L&M: Lower & Middle Allochthons; U: Upper Allochthon; Um: Uppermost Allochthon. (b) Structural map of the study area. The red star shows the location of the studied sample from Vågsvåg on the Vågsøy island (WGS84: 61.93106N, 5.05121E) with the approximate peak *P*–*T* conditions inferred from our study. Approximate peak temperatures after Kylander-Clark et al. (2008), peak pressures after Hacker et al. (2010) and eclogite locations after Young (2018). (c) Schematic cross-section modified after Labrousse (2001) and Johnston, Hacker, & Andersen (2007). NSDZ: Nordfjord-Sogn Detachment Zone; HD: Hornelen Detachment. Locations referred to in the text are Flatraket (F), Kråkeneset (K), the Stadlandet peninsula (S), Drage (D), Verpeneset (V), Ulvesund (U) and Eiksunddal (E).

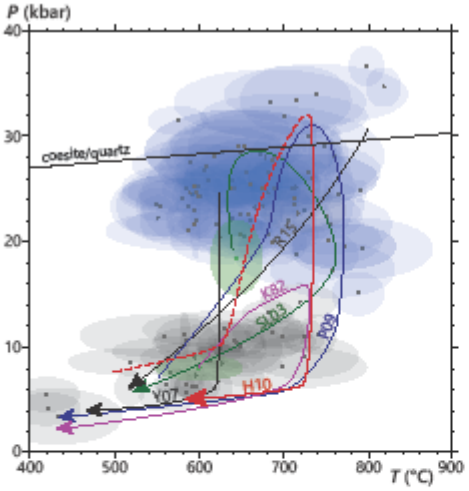

Figure 2. Summary of P–T paths in the Nordfjord-Stadlandet (U)HP zone from Krogh (1982; K82), Schärer & Labrousse (2003; SL03), Young et al. (2007; Y07), Peterman et al. (2009; P09) and Renedo et al. (2015; R15). Schematic P–T path for the UHP zones of the WGR from Hacker et al. (2010; H10). Compilation of P–T conditions in the same area for eclogites (blue ellipses), gneisses, amphibolites and retrogressed eclogites (grey ellipses) and for pre-eclogite relics (green ellipses) from Krogh (1982), Cuthbert et al. (2000), Wain et al. (2001), Labrousse et al. (2004), Hacker (2006), Anderson & Moecher (2007), Johnston, Hacker, & Ducea (2007), Young et al. (2007), Peterman et al. (2009) and Medaris et al. (2018).

Figure 2. Summary of *P–T* paths in the Nordfjord-Stadlandet (U)HP zone from Krogh (1982; K82), Schärer & Labrousse (2003; SL03), Young et al. (2007; Y07), Peterman et al. (2009; P09) and Renedo

et al. (2015; R15). Schematic *P*–*T* path for the UHP zones of the WGR from Hacker et al. (2010; H10). Compilation of *P*–*T* conditions in the same area for eclogites (blue ellipses), gneisses, amphibolites and retrogressed eclogites (grey ellipses) and for pre-eclogite relics (green ellipses) from Krogh (1982), Cuthbert et al. (2000), Wain et al. (2001), Labrousse et al. (2004), Hacker (2006), Anderson & Moecher (2007), Johnston, Hacker, & Ducea (2007), Young et al. (2007), Peterman et al. (2009) and Medaris et al. (2018).

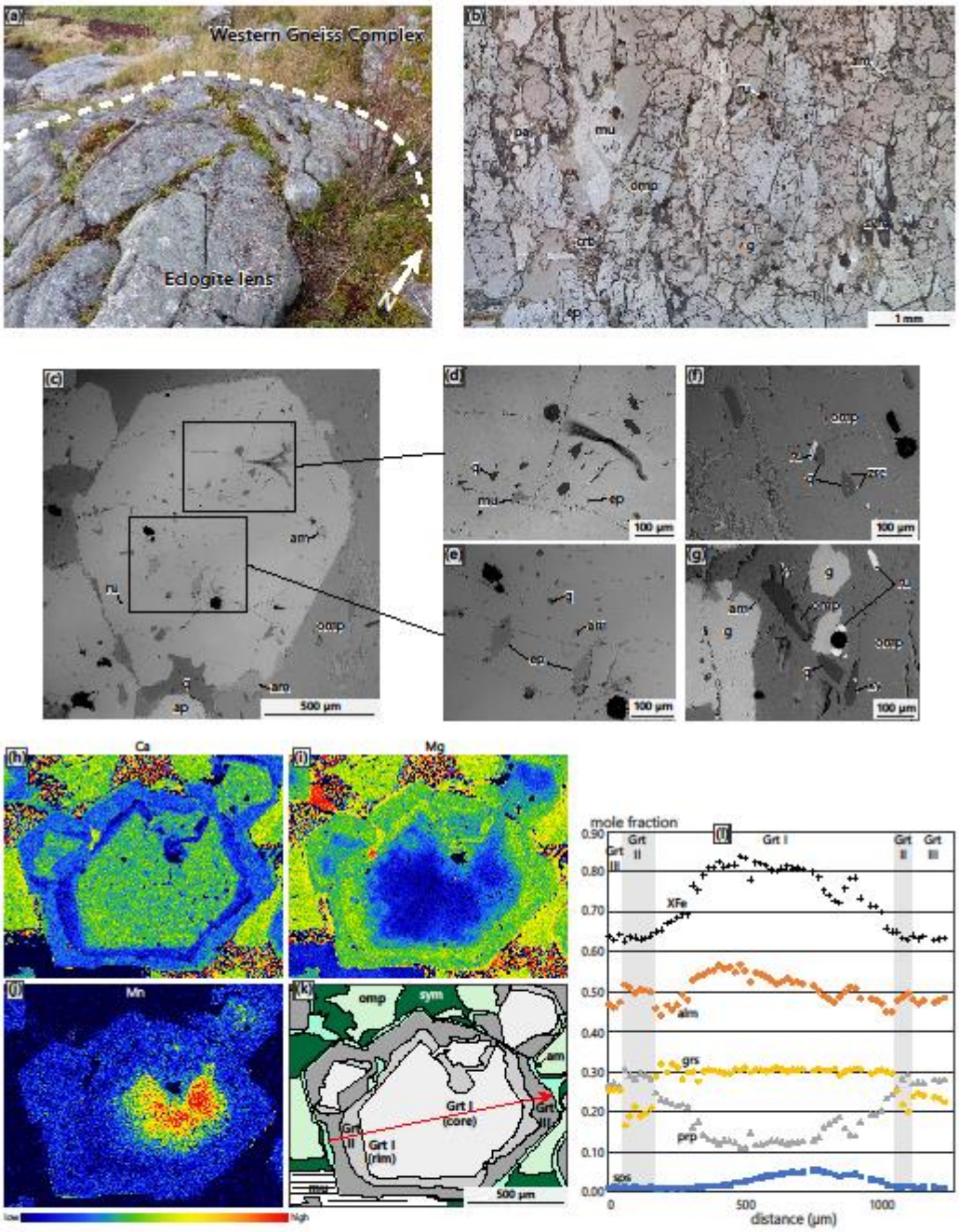

Figure 3. Eclogite lens sampled near the Vågsberget museum, hammer for scale (a). Photomicrograph (plane polarized light) of eclogite sample NO7A (b). BSE image of garnet (c) and zooms on inclusions (d–e). BSE images of inclusions in omphacite (f–g). X-ray chemical maps for Ca (h), Mg (i) and Mn (j). (k) Hand drawing of the same garnet as in (h–j) with the garnet growth zones highlighted. (l) Chemical profile of garnet located by the red arrow in (k).

Figure 3. Eclogite lens sampled near the Vågsberget museum, hammer for scale (a). Photomicrograph (plane polarized light) of eclogite sample NO7A (b). BSE image of garnet (c) and

zooms on inclusions (d–e). BSE images of inclusions in omphacite (f–g). X-ray chemical maps for Ca (h), Mg (i) and Mn (j) showing the chemical zoning of garnet. (k) Hand drawing of the same garnet as in (h–j) with the garnet growth zones highlighted. (l) Chemical profile of garnet located by the red arrow in (k).

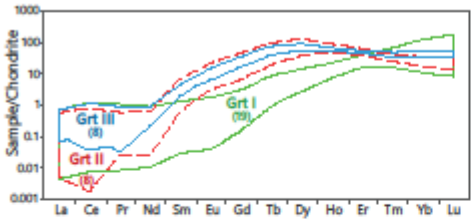

Figure 4. REE spidergram for garnet. Analyses are normalized to chondritic values (Sun & McDonough, 1989). Number of analyses for each garnet zone in brackets.

Figure 4. REE spidergram for garnet. Analyses are normalized to chondritic values (Sun & McDonough, 1989). Number of analyses for each garnet zone in brackets.

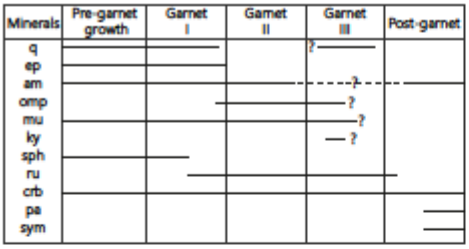

Figure 5. Paragenetic sequence for eclogite sample NO7A.

Figure 5. Paragenetic sequence for eclogite sample NO7A.

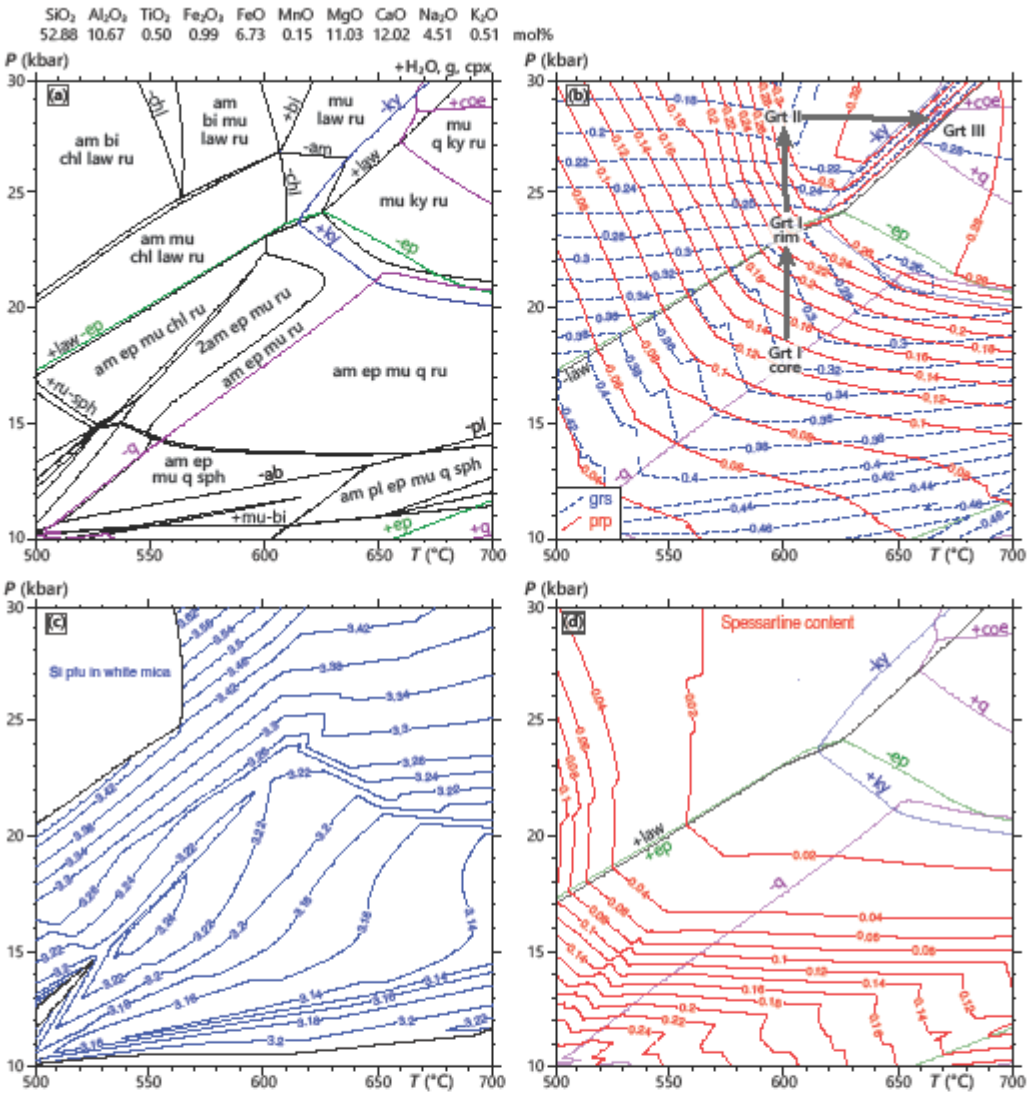

Figure 6. P–T pseudosections for eclogite sample NO7A calculated for the indicated bulk composition (H2O is considered in excess). Some small fields are unlabelled for clarity. Grey arrows indicate the inferred P–T path. Kyanite, quartz/coesite, epidote and lawsonite stability fields reported in (b) and (d) as in (a). See text for further details.

Figure 6. *P–T* pseudosections for eclogite sample NO7A calculated for the indicated bulk composition (H_2O is considered in excess). Some small fields are unlabelled for clarity. Grey arrows

indicate the inferred *P*–*T* path. Kyanite, quartz/coesite, epidote and lawsonite stability fields reported in (b) and (d) as in (a). See text for further details.

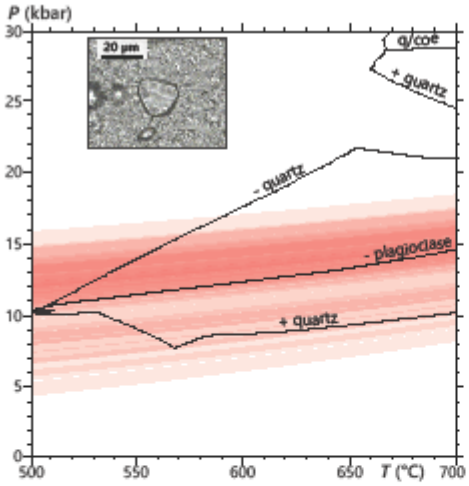

Figure 7. *P–T* diagram of quartz entrapment conditions. Isomekes are represented by the red areas; the width of which corresponds to the associated uncertainty. Stronger colour denotes overlapping results. Stability fields of plagioclase and quartz/coesite as in Figure 6a; garnet is stable throughout the *P–T* range. Inset: photomicrograph of a typical quartz inclusion analysed by Raman spectroscopy.

Figure 7. *P–T* diagram of quartz entrapment conditions. Isomekes are represented by the red areas, the width of which corresponds to the associated uncertainty. Stronger colour denotes overlapping

results. Stability fields of plagioclase and quartz/coesite as in Figure 6a; garnet is stable throughout the *P*–*T* range. Inset: photomicrograph of a typical quartz inclusion analysed by Raman spectroscopy.

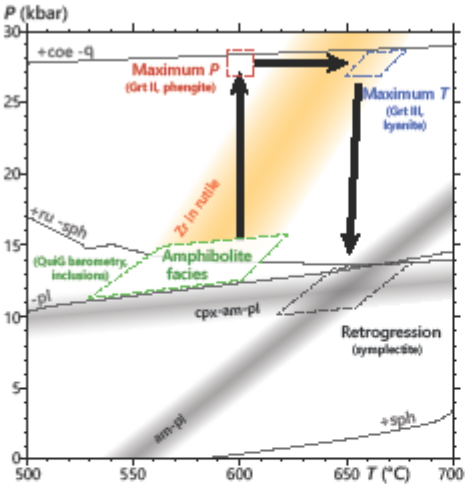

Figure 8. Schematic *P–T* evolution inferred for the Vågsøy eclogite. Plagioclase, rutile and titanite stability fields as in Figure 6a. The red and blue boxes represent the P–T field inferred from the intersection of garnet isopleths. Zr-in-rutile thermometry results using the calibration of Tomkins et al. (2007), amphibole-plagioclase thermobarometry using the calibration of Holland & Blundy (1994) and clinopyroxene-amphibole-plagioclase thermobarometry from THERMOCALC average P calculations, represented with their 1 sigma uncertainty.

Figure 8. Schematic *P–T* evolution inferred for the Vågsøy eclogite. Plagioclase, rutile and titanite stability fields as in Figure 6a. The red and blue boxes represent the *P–T* conditions inferred from the

intersection of garnet isopleths. Zr-in-rutile thermometry results using the calibration of Tomkins et al. (2007), amphibole-plagioclase thermobarometry using the calibration of Holland & Blundy (1994) and clinopyroxene-amphibole-plagioclase thermobarometry from THERMOCALC average P calculations, represented with their 1 sigma uncertainty.

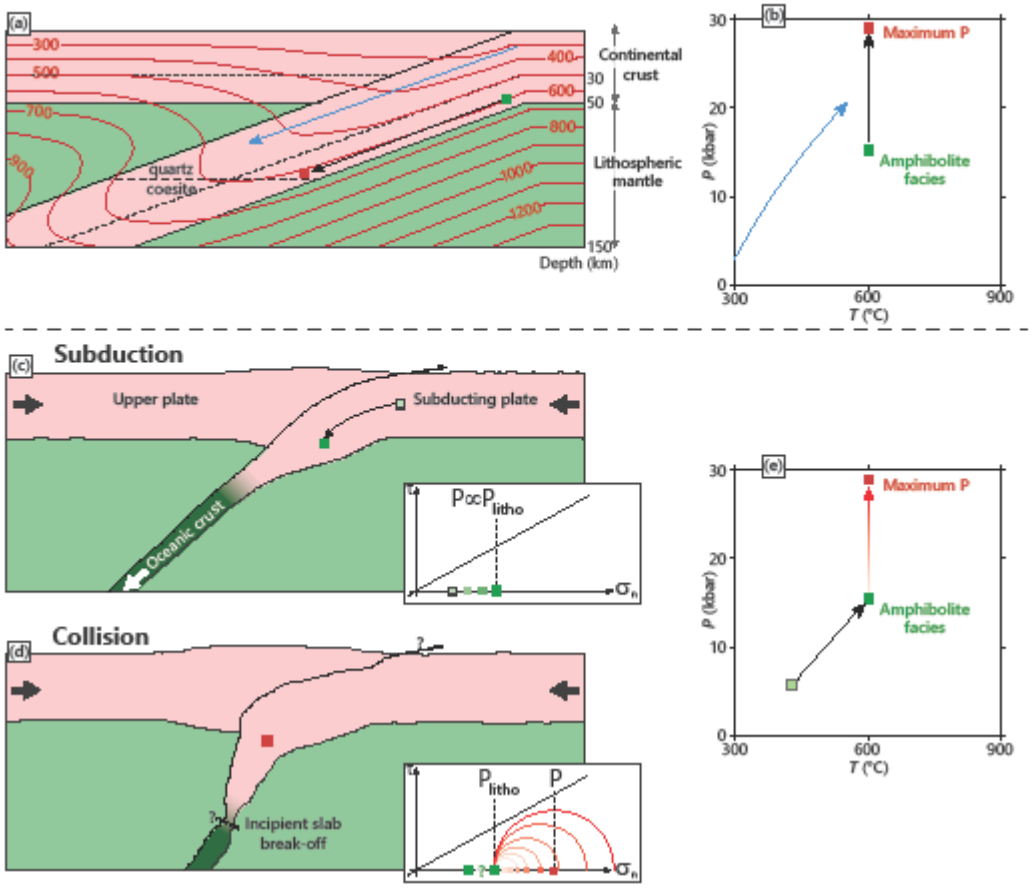

Figure 9. Possible geodynamic scenarios for the studied eclogite. (a) Thermal steady state of a subduction zone. Isotherms (in °C) are after the modelling of Fauconnier et al. (2014), initially carried out for a 30 km thick crust (dashed line). (b) *P*–*T* evolution for the markers (i.e., blue arrow, green and red points) depicted in (a). Pressure is reported in this diagram by converting depth from (a) into pressure assuming pressure as lithostatic only and by considering an average rock density of 2700 kg·m^{-3}. (c–d) Schematic tectonic history with initiation of continental subduction (c) and subsequent collision (d). Mohr diagrams for each stage are displayed in insets. P_{litho} denotes lithostatic pressure, τ and σ_n correspond to shear stress and normal stress, respectively. The black line represents the Mohr-Coulomb yield criteria. (e) *P*–*T* evolution for the tracers in (c–d). Boxes (a, c–d) are 150x400 km large, same vertical and horizontal scale. In (c–d), crust is 45 km thick, as suggested by Kylander-Clark et al. (2009) and the reconstructions of Hacker et al. (2010).

Figure 9. Possible geodynamic scenarios for the studied eclogite. (a) Thermal steady state of a subduction zone. Isotherms (in °C) are after the modelling of Fauconnier et al. (2014), initially carried

out for a 30 km thick crust (dashed line). (b) *P–T* evolution for the markers (i.e., blue arrow, green and red points) depicted in (a). Pressure is reported in this diagram by converting depth from (a) into pressure assuming pressure as lithostatic only and by considering an average rock density of 2700 $kg \cdot m^{-3}$. (c–d) Schematic tectonic history with initiation of continental subduction (c) and subsequent collision (d). Mohr diagrams for each stage are displayed in insets. P_{litho} denotes lithostatic pressure, τ and σ_n correspond to shear stress and normal stress, respectively. The black line represents the Mohr-Coulomb yield criteria. (e) *P–T* evolution for the tracers in (c–d). Boxes (a, c–d) are 150x400 km large, same vertical and horizontal scale. In (c–d), crust is 45 km thick, as suggested by Kylander-Clark et al. (2009) and the reconstructions of Hacker et al. (2010).